


# Two-step structural changes in M3 muscarinic receptor activation rely on the coupled $G_q$ protein cycle

Received: 30 July 2022

Yong-Seok Kim<sup>1</sup>, Jun-Hee Yeon<sup>1</sup>, Woori Ko<sup>1</sup> & Byung-Chang Suh<sup>1</sup>✉

Accepted: 23 February 2023

Published online: 08 March 2023

 Check for updates

G protein-coupled receptors (GPCRs) regulate diverse intracellular signaling pathways through the activation of heterotrimeric G proteins. However, the effects of the sequential activation–deactivation cycle of G protein on the conformational changes of GPCRs remains unknown. By developing a Förster resonance energy transfer (FRET) tool for human M3 muscarinic receptor (hM3R), we find that a single-receptor FRET probe can display the consecutive structural conversion of a receptor by G protein cycle. Our results reveal that the G protein activation evokes a two-step change in the hM3R structure, including the fast step mediated by  $G_q$  protein binding and the subsequent slower step mediated by the physical separation of the  $G\alpha_q$  and  $G\beta\gamma$  subunits. We also find that the separated  $G\alpha_q$ -GTP forms a stable complex with the ligand-activated hM3R and phospholipase  $C\beta$ . In sum, the present study uncovers the real-time conformational dynamics of innate hM3R during the downstream  $G_q$  protein cycle.

G protein-coupled receptors (GPCRs) are one of the largest families of membrane receptors, with more than 800 members encoded by about 3% of human genes<sup>1–3</sup>. They are widely expressed in cells organizing tissues and organs, and regulate cellular and physiological processes by transmitting various extracellular signals, including light, temperature, neurotransmitters, hormones, and odor substances, into cells<sup>4,5</sup>. The GPCR signals are transmitted to membrane-associated effectors like ion channels and enzymes through several heterotrimeric ( $G\alpha\beta\gamma$ ) G proteins. As mediators, G proteins play an important role in enabling GPCR signaling to have high flexibility, sensitivity, and specificity<sup>5</sup>. For this reason, the way in which GPCRs and G proteins interact with each other to induce this signaling efficiency in living cells has been studied extensively<sup>6–8</sup>.

When GPCRs are activated by an agonist, the receptors combine with inactive heterotrimeric G proteins, followed by GDP release from the  $G\alpha$  subunit and GTP binding to the site, leading to the transient stabilization of the GPCR–G protein complexes<sup>9</sup>. Through biochemical and biophysiological methods, the interaction sites of these active-state GPCR–G protein complexes have been clarified in terms of the relationships between GPCR and  $G\alpha$ <sup>10–12</sup>, GPCR and  $G\beta\gamma$ <sup>13–16</sup>, and  $G\alpha$  and

$G\beta\gamma$ <sup>10,17,18</sup>. In more recent studies, high resolution structures of those complexes have been defined by cryogenic electron microscopy<sup>19–25</sup>.

Although they have been less studied compared with the active-state GPCR–G protein complexes, some resting-state complexes called preassembled inactive-state complexes have also been explored recently using ligand-binding and biochemical studies<sup>24,26–28</sup> as well as biophysical studies in live cells<sup>29–33</sup>. These studies suggested that the preassembled complex formation may accelerate the onset of signaling by GPCRs and thus increase the GPCR sensitivity<sup>33</sup>. However, it has not yet been determined which subunit of heterotrimeric G proteins interacts with GPCRs in their preassembly or whether the preassembly is maintained during the receptor activation without further structural changes. Moreover, some studies have looked into the different receptor conformations during the different stages of the G protein activation cycle<sup>34,35</sup>, though the real-time effects of the G protein activation cycle on the innate conformation of GPCR remain unknown.

In this study, we develop a Förster resonance energy transfer (FRET) construct of human muscarinic acetylcholine receptor M3, hM3R-YFP-CFP, which enables the analysis of the conformational transition of hM3R that occurs during the coupled  $G_q$  protein cycling

<sup>1</sup>Department of Brain Sciences, Daegu Gyeongbuk Institute of Science and Technology (DGIST), Daegu 42988, Republic of Korea.

✉ e-mail: [bcsuh@dgist.ac.kr](mailto:bcsuh@dgist.ac.kr)

processes as well as the cascade from hM3R to phospholipase C $\beta$  (PLC $\beta$ ) within cells. Using this FRET construct, we find that the activation–deactivation cycle of G $_q$  protein evokes multistep conformational changes of hM3R, which depend on the time-dependent association, separation, and dissociation of G $_q$  protein subunits. We also provide evidence that the separated G $\alpha_q$  and G $\beta\gamma$  subunits continuously stay on the agonist-activated hM3R, steadily activate PLC $\beta$ , and release from the receptor with different time constants. Our results demonstrate that the downstream G $_q$  protein cycle inversely and dynamically regulates the upstream hM3R structure.

## Results

### A single hM3R-YFP-CFP FRET construct revealed a two-step hM3R activation signal

To investigate the signaling properties of M3R, a hM3R FRET construct, hM3R-YFP-CFP was constructed by replacing the third intracellular loop (ICL3) of wild-type hM3R with YFP and tagging CFP to the C-terminus (Fig. 1a) without damaging the selective recognition sites of G $_{q/11}$ -proteins (Supplementary Fig. 1a–c). The receptor was activated by applying the muscarinic receptor agonist oxotremorine-M (Oxo-M). In contrast to the previously reported mouse M1 muscarinic FRET probe (mM1R-YFP-CFP)<sup>36</sup>, binding of Oxo-M to this hM3R-YFP-CFP decreased the FRET ratio (FRET $r$ ) signal (Fig. 1b). In addition, hM3R-YFP-CFP showed ~3-fold larger FRET $r$  responses and a ~5-fold higher signal-to-noise ratio (SNR) compared to mM1R-YFP-CFP (Fig. 1b–d). Photostability was also improved, and thus, the FRET $r$  signal was maintained longer without a significant decrease compared to mM1R-YFP-CFP (Supplementary Fig. 1d, e). When the FRET $r$  of the hM3R-YFP-CFP construct was measured in intact HEK293T cells under the faster perfusion system with higher frequency ( $f=10$  Hz), we found a two-step reduction of the FRET $r$  signal with faster (step 1) and then slower (step 2) responses by Oxo-M treatment (Fig. 1e, top). There was a short delay ( $0.08 \pm 0.05$  s,  $n=5$ ) before the step 1. The time constant  $\tau$  values of step 1 and step 2 were  $0.22 \pm 0.02$  s and  $1.92 \pm 0.30$  s ( $n=5$ ), respectively (Fig. 1f, top). However, the relative responsiveness of the two steps was almost equal at around 50% (Fig. 1g, top). Elevation of the sampling frequency to 100 Hz decreased the photostability but did not divide steps 1 and 2 further (Supplementary Fig. 1f). The FRET $r$  change of the receptor was also measured after the application of the natural ligand acetylcholine (ACh). Consistent with the data of Oxo-M, 1  $\mu$ M ACh induced two-step activation of hM3R-YFP-CFP with faster step 1 and slower step 2 responses (Fig. 1e–g, bottom). Both Oxo-M and ACh changed the FRET $r$  signal in a concentration-dependent manner, but with significantly different EC $_{50}$  values of 0.007  $\mu$ M for ACh and 0.112  $\mu$ M for Oxo-M (Supplementary Fig. 2). The results suggest that ACh had a higher affinity for hM3R-YFP-CFP receptor compared to Oxo-M, which was similar to the responses of other M3R FRET sensors<sup>37</sup>.

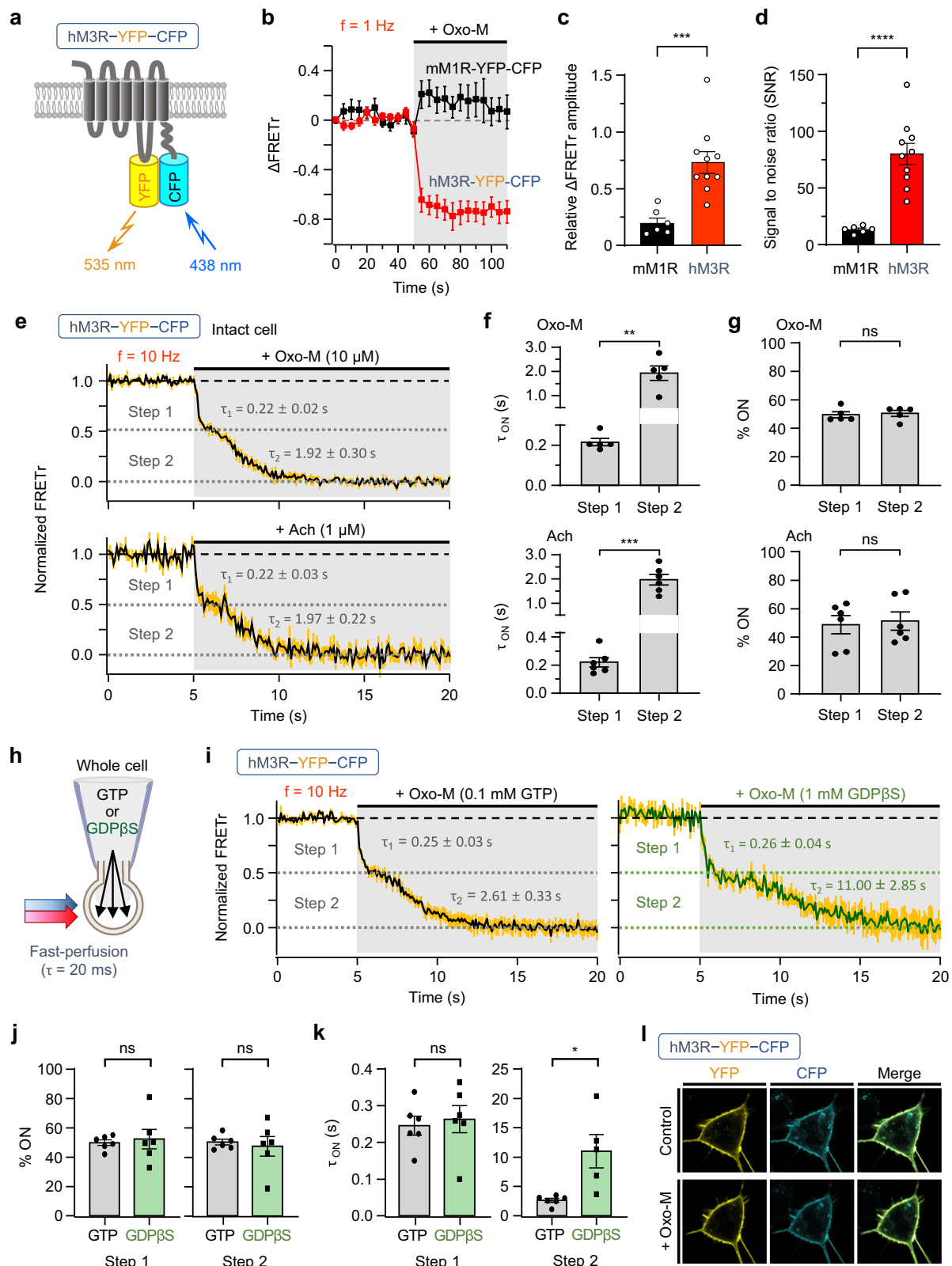
To characterize the two steps of the hM3R-YFP-CFP FRET response, we manipulated intracellular GTP concentrations in the whole-cell configuration of the cells (Fig. 1h). In cells intracellularly perfused with the physiological level of GTP (0.1 mM), Oxo-M application induced almost the same two-step reduction in the FRET $r$  signal of hM3R-YFP-CFP as those of intact cells (Fig. 1i, left). The cells patched with a pipette solution containing 1 mM of the GDP analog guanosine 5-O-(2-thiodiphosphate) (GDP $\beta$ S) as a competitive antagonist of GTP binding to G proteins also displayed a two-step FRET $r$  reduction with a similar proportion of step 1 and step 2 in the overall response (Fig. 1i, right, j). The time constant of the step 1 response was not changed, but the response of step 2 was nearly 5 times slower than that of cells with 0.1 mM of GTP (Fig. 1k). These results suggest that step 1 is likely related to the conformational change following the activation of hM3R-YFP-CFP by agonist binding, while step 2 represents the additional conformational changes of the receptor following the G protein activation. To check whether the internalization of the receptor affects

the FRET $r$  change, hM3R-YFP-CFP expression on the HEK293T cell membrane was visualized with a confocal microscope. We confirmed that there were no detectable changes in the fluorescence distribution of hM3R-YFP-CFP at the plasma membrane before and after the receptor activation (Fig. 1l).

To examine whether Oxo-M binding to hM3R-YFP-CFP normally evokes downstream intracellular signaling through the activation of coupled G $_q$  protein, PLC-mediated hydrolysis of phosphatidylinositol 4,5-bisphosphate (PIP $_2$ ) was measured in cells co-transfected with the PIP $_2$  probe RFP-labeled pleckstrin homology domain of PLC $\delta_1$  (RFP-PH). Cells transfected with the wild-type mM1R or hM3R plasmid showed a strong translocation of RFP-PH from the plasma membrane to cytosol by Oxo-M treatment (Supplementary Fig. 3a–c). There was no significant movement of RFP-PH in cells expressing mM1R-YFP-CFP, confirming that mM1R-YFP-CFP cannot trigger downstream signaling pathways, as reported in a previous study<sup>36</sup> (Supplementary Fig. 3d). However, Oxo-M induced strong translocation of RFP-PH in cells expressing hM3R-YFP-CFP, suggesting that the activation of hM3R-YFP-CFP by Oxo-M can stimulate downstream signaling pathways through G $_q$  protein activation (Supplementary Fig. 3e). There was a slight difference in the relative RFP-PH changes at the plasma membrane and cytosol, but the half time of activation ( $T_{50}$ ) showed very similar kinetics to those of wild-type hM3R (Supplementary Fig. 3f, g). Those results were further confirmed in the experiments with ACh (Supplementary Fig. 4a, b). Though there was a considerable decrease in the relative fluorescence changes at the PM and cytosol (Supplementary Fig. 4c), the kinetics for the PIP $_2$  hydrolysis were not changed in the FRET receptor (Supplementary Fig. 4d). Therefore, the results suggest that hM3R-YFP-CFP can transmit external signals to downstream pathways through the activation of the G $_q$  protein with similar kinetics to that of wild-type hM3R.

### Two-step activation of hM3R-YFP-CFP can be explained by G $_q$ protein activation

Based on the similarity between hM3R-YFP-CFP and wild-type hM3R in terms of kinetics of PIP $_2$  depletion, we further examined the molecular basis of the two steps. First, we hypothesized that the pathways corresponding to the fast step 1 of hM3R-YFP-CFP were related to a conformational change following Oxo-M binding to the receptor and subsequent interaction of the activated receptor with the heterotrimeric G $_q$  protein. Thus, we performed FRET experiments in cells transfected with hM3R-CFP, G $\beta_1$ -YFP, and cognate G protein subunits (Fig. 2a). The results showed a single-step FRET $r$  response composed of a fast signal upon Oxo-M treatment as reported in previous G $_q$ -coupled receptors<sup>36,38</sup> (Fig. 2b, left, c, gray). The  $\tau$  of the step ( $0.23 \pm 0.04$  s) (Fig. 2d, gray) was very similar to the step 1  $\tau$  of hM3R-YFP-CFP (Fig. 1k, left, gray), suggesting that the step 1 reaction includes fast coupling between hM3R and G $_q$  protein after Oxo-M binding to the receptor. We conducted the same experiment yet 0.1 mM of GTP in the pipette solution was replaced with 1 mM of GDP $\beta$ S to cross-check the similarity between the responses (Fig. 2b, right). The results showed that there was also a single FRET $r$  signal response with almost the same time constant as that with 0.1 mM GTP (Fig. 2c, d, green) or step 1 reaction of hM3R-YFP-CFP (Fig. 1k, left), confirming that intracellular GTP concentration does not affect the step 1 reaction. We also measured the difference in the SNR of step 1 between hM3R-YFP-CFP and hM3R-CFP plus G $\beta_1$ -YFP (Fig. 2e). The SNR value ( $169 \pm 23$ ) of the step 1 response of hM3R-YFP-CFP was nearly twice those of hM3R-CFP plus G $\beta_1$ -YFP with 0.1 mM of GTP ( $90 \pm 14$ ) or with 1 mM of GDP $\beta$ S ( $69 \pm 8$ ) (Fig. 2e; Supplementary Fig. 5a, b). There was no significant difference in the SNR between cells intracellularly perfused with GTP or GDP $\beta$ S. Finally, Oxo-M induced the coupling of hM3R-CFP and G $\beta_1$ -YFP in a concentration-dependent manner with the EC $_{50}$  value of ~2  $\mu$ M (Supplementary Fig. 6a, c). When we measured the coupling between



G $\beta$ 1-YFP and hM3R-BFP-CFP where the YFP was replaced by blue fluorescence protein (BFP), there was no significant change in the EC<sub>50</sub> value (Supplementary Fig. 6b, c). The  $\tau_{ON}$  value was not changed, but the SNR level decreased because of the partial reduction in the FRET signal amplitude (Supplementary Fig. 6d). These results suggest that the insertion of YFP to the ICL3 could attenuate the potency for the G<sub>q</sub> protein coupling to our M3R FRET reporter.

We also performed FRET experiments between G $\alpha_q$  and G $\beta$  subunits in cells expressing G $\alpha_q$ -CFP and G $\beta$ 1-YFP with wild-type hM3R, Gy2, and GRK2 (Fig. 2f). GRK2 has been known to interact with G<sub>q</sub> protein subunits<sup>39,40</sup> to regulate the downstream signaling pathways. The results showed a single-step reduction of FRETr with  $0.25 \pm 0.08$ -s delay ( $n = 6$ ) upon Oxo-M treatment (Fig. 2g, left, h, gray). The average  $\tau$  value of this step was  $1.45 \pm 0.19$  s (Fig. 2i gray), which

**Fig. 1 | hM3R-YFP-CFP FRET construct shows a two-step activation.** **a** Schematic of double-labeled hM3R construct hM3R-YFP-CFP at the plasma membrane. **b**  $\Delta$ FRET<sub>r</sub> signal (**b**), relative  $\Delta$ FRET<sub>r</sub> amplitude (**c**) and SNR (**d**) in response to Oxo-M in cells expressing mMIR-YFP-CFP or hM3R-YFP-CFP. Sampling frequency: 1 Hz. mM3R,  $n = 6$  (three cultures); hM3R,  $n = 10$  (four cultures). Welch's  $t$  test (two-sided,  $^{***}p = 0.0003$ ,  $^{****}p < 0.0001$ ). **e** Normalized FRET<sub>r</sub> signals in response to Oxo-M (top) or acetylcholine (Ach, bottom) in intact cell expressing hM3R-YFP-CFP. The FRET<sub>r</sub> changes from Oxo-M or Ach application show two-step activation decay in intact cells. Sampling frequency: 10 Hz. Yellow vertical lines indicate SEM.  $n = 5$  (two cultures, top);  $n = 6$  (two cultures, bottom). Time constant ( $\tau_{ON}$ ) (**f**) and percent distribution (**g**) of each activation step in total FRET<sub>r</sub> response in intact cells treated with each agonist. Oxo-M,  $n = 5$  (two cultures, Mann–Whitney test, two-sided,

$^{**}p = 0.0079$ ); Ach,  $n = 6$  (two cultures, Welch's  $t$  test, two-sided,  $^{***}p = 0.0004$ ). **h** Whole-cell configuration of a cell with internal pipette solution containing 0.1 mM GTP or 1 mM GDP $\beta$ S. **i** Two-step activation decay of FRET<sub>r</sub> by Oxo-M application in cells intracellularly perfused with 0.1 mM GTP (left) or 1 mM GDP $\beta$ S (right). Sampling frequency: 10 Hz. Yellow vertical lines indicate SEM. GTP,  $n = 6$  (three cultures); GDP $\beta$ S,  $n = 6$  (two cultures). Percent distribution (**j**) and  $\tau_{ON}$  (**k**) of each step in the FRET<sub>r</sub> response under patched conditions. GTP,  $n = 6$  (three cultures); GDP $\beta$ S,  $n = 6$  (two cultures). Welch's  $t$  test (two-sided,  $^{*}p = 0.0416$ ). **l** Representative confocal images of a single cell expressing hM3R-YFP-CFP before (Control) and during Oxo-M application (+ Oxo-M). Experiments repeated independently for more than five cultures show similar results. Scale bar, 10  $\mu$ m. Data are shown as mean  $\pm$  SEM. ns not significant. Source data are provided as a Source Data file.

was similar to that of the step 2 response of hM3R-YFP-CFP (Fig. 1k, right, gray). We conducted the same experiment in the presence of 1 mM of GDP $\beta$ S instead of GTP (Fig. 2g, right). The results showed that with GDP $\beta$ S, the response was much slower ( $10.38 \pm 1.46$  s) (Fig. 2i, green) compared to that of cells with GTP (Fig. 2i, gray) but similar to that of the step 2 response of hM3R-YFP-CFP with GDP $\beta$ S (Fig. 1k, right, green). We also found that there was no significant difference in the SNR between hM3R-YFP-CFP (step 2) and  $G\alpha_q$ -CFP plus  $G\beta_1$ -YFP under the GTP or GDP $\beta$ S condition (Fig. 2j; Supplementary Fig. 5c, d), suggesting that the step 2 FRET response of hM3R-YFP-CFP corresponds to the slow dissociation of  $G\alpha_q$  and  $G\beta$  subunits after activation on the receptor. Using confocal microscopy we confirmed that the cells expressing hM3R-CFP plus  $G\beta_1$ -YFP or  $G\alpha_q$ -CFP plus  $G\beta_1$ -YFP showed normal PIP<sub>2</sub> hydrolysis through  $G_q$  protein activation (Supplementary Fig. 7a, c and 7b, d, bottom). Moreover, hM3R activation did not release any  $G\alpha_q$  and  $G\beta$  subunits from the plasma membrane to the cytosol (Supplementary Fig. 7a, c and 7b, d, top), suggesting that both subunits were independently tethered to the plasma membrane after separation.

### Oxo-M dissociation evoked two-step deactivation kinetics in hM3R-YFP-CFP

We also measured the deactivation kinetics of hM3R-YFP-CFP after Oxo-M washout. As shown in Supplementary Fig. 8a, hM3R-YFP-CFP deactivation showed a two-step FRET<sub>r</sub> recovery with faster step 1 and slower step 2 reactions. To determine the nature of these two steps, FRET<sub>r</sub> was also measured during the receptor deactivation in cells expressing hM3R-CFP plus  $G\beta_1$ -YFP or  $G\alpha_q$ -CFP plus  $G\beta_1$ -YFP (Supplementary Fig. 8b, c). As a result, the deactivations were observed as a single step in both experiments. The deactivation  $\tau$  of hM3R-CFP plus  $G\beta_1$ -YFP ( $0.53 \pm 0.04$  s) showed a value very similar to that of step 1 ( $0.47 \pm 0.08$  s) of hM3R-YFP-CFP deactivation (Supplementary Fig. 8d), whereas that of  $G\alpha_q$ -CFP plus  $G\beta_1$ -YFP ( $21.37 \pm 1.34$  s) was similar to that of step 2 ( $20.02 \pm 2.29$  s) of hM3R-YFP-CFP deactivation (Supplementary Fig. 8e). In terms of percent distribution of each step in the total recovery, both hM3R-CFP plus  $G\beta_1$ -YFP and  $G\alpha_q$ -CFP plus  $G\beta_1$ -YFP showed a similar distribution value of around 88% (Supplementary Fig. 8f, g). We further confirmed that, consistent with previous findings<sup>36</sup>, the coexpression of GRK2 significantly increased the signal amplitude and SNR of the FRET<sub>r</sub> response between  $G\alpha_q$ -CFP and  $G\beta_1$ -YFP but did not change the kinetics of receptor-induced activation or deactivation (Supplementary Fig. 9). GRK2 expression neither affect the kinetics nor the peak responses of FRET<sub>r</sub> in hM3R-YFP-CFP, but decreased the SNR by slightly enhancing the noise level (Supplementary Fig. 10).

### hM3R-YFP-CFP can make a complex with the separated $G\beta$ subunits

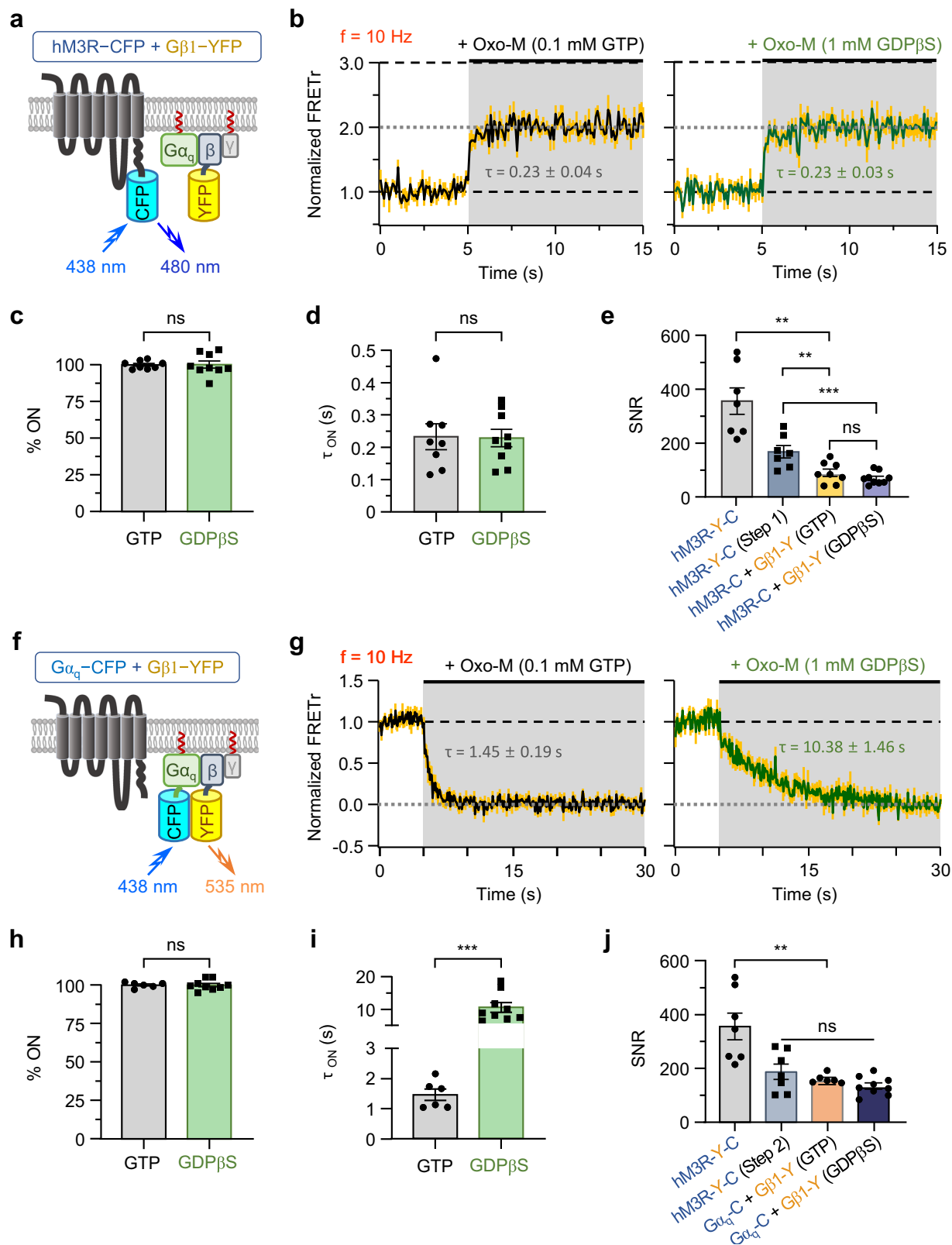
To further elucidate how hM3R communicates with  $G_q$  proteins to transmit external signals to the downstream pathways, we constructed two constitutively active  $G\alpha_q$  mutant forms:  $G\alpha_q(Q209L)$  and  $G\alpha_q(R183C)$  (Fig. 3a). Previous studies have reported that diseases such

as uveal melanoma result from continuous GPCR activity through  $G\alpha_q$  mutation (Q209L or R183C) and loss of GTPase activity of the subunit<sup>41–43</sup>. First, we examined if the additional expression of wild-type  $G_q$  proteins affects the Oxo-M-induced FRET<sub>r</sub> signal of hM3R-YFP-CFP (Supplementary Fig. 11). As shown in Fig. 3b and Supplementary Fig. 12, the overexpression of wild-type  $G_q$  proteins did not change the two-step kinetics for activation and deactivation, the percentage recovered, or the SNR of hM3R-YFP-CFP. However, in cells co-transfected with mutant  $G\alpha_q(Q209L)$  or  $R183C$  and cognate G protein subunits, only a single step of activation and recovery was identified in the FRET<sub>r</sub> experiment (Fig. 3c), showing a comparable time constant to step 1 (ON or OFF) of wild-type  $G_q$  protein (Fig. 3d). Because of the absence of step 2, the FRET<sub>r</sub> was almost completely recovered within a single step (Fig. 3e). Consistently, after the intracellular perfusion of the nonhydrolyzable GTP analog guanosine 5-O-(3-thiotriphosphate) (GTP $\gamma$ S), Oxo-M evoked a single-step activation of FRET<sub>r</sub> probably because GTP $\gamma$ S activated the G proteins almost irreversibly<sup>44</sup> (Supplementary Fig. 13).

Next, we performed the FRET<sub>r</sub> experiment between hM3R-CFP and  $G\beta_1$ -YFP in cells co-expressing mutant  $G\alpha_q(Q209L)$  or  $R183C$  and Gy2. The results showed that Oxo-M induced a single-step FRET<sub>r</sub> change with similar time constants and percentage recovered, but significantly lower SNR compared to those of wild-type  $G\alpha_q$  (Fig. 3f–h; Supplementary Fig. 14). These results suggest that, upon Oxo-M binding to the receptor, hM3R can independently interact with the separated  $G\beta$  subunits though its binding affinity is weaker than that for heterotrimeric G protein. Interestingly, the results also showed that the interaction between the hM3R and  $G\beta$  subunit was sustained during the application of the agonist and recovered immediately after Oxo-M washout. Finally, a FRET<sub>r</sub> experiment was performed in cells expressing hM3R, mutant  $G\alpha_q(Q209L)$  or  $R183C$ -CFP,  $G\beta_1$ -YFP, Gy2, and GRK2. The results showed no changes in FRET<sub>r</sub> by Oxo-M application, except in wild-type  $G\alpha_q$  (Fig. 3i–k), indicating that the mutant  $G\alpha_q(Q209L)$  or  $R183C$  and  $G\beta$  subunits were dissociated in the resting condition and thus responded to receptor activation separately.

### Inhibition of GDP release from $G\alpha_q$ selectively blocked the step 2 response of hM3R-YFP-CFP

YM-254890 (YM) has been studied as a candidate drug for diverse diseases, such as thrombosis, asthma, and melanoma<sup>43</sup>. Preclinical studies have shown that YM's main mechanism of action is the inhibition of GDP release from the  $G\alpha_q$  protein<sup>43</sup>. We examined the effects of YM on the FRET<sub>r</sub> response of the hM3R and  $G_q$  proteins. As seen in Fig. 4a, left, in the presence of YM, only the step 1 (ON and OFF) FRET<sub>r</sub> response was detected upon Oxo-M application in cells expressing hM3R-YFP-CFP and wild-type  $G_q$  proteins. When the YM was removed in the middle of hM3R-YFP-CFP activation with Oxo-M, the cells showed a slow step 2<sub>ON</sub> FRET<sub>r</sub> response up to about 31% of the total FRET<sub>r</sub> activation (step 1<sub>ON</sub> + step 2<sub>ON</sub>) and a step 2<sub>OFF</sub> response up to about 30% of the total deactivation (step 1<sub>OFF</sub> + step 2<sub>OFF</sub>) (Fig. 4a, b, red). However, the results of experiments with mutant  $G\alpha_q(Q209L)$  revealed that there was a normal step 1 FRET<sub>r</sub> response by Oxo-M but



that the step 2 response was not detected in hM3R-YFP-CFP even after washing out YM (Fig. 4c, d). This could have been due to the pre-separation of constitutively active mutant G $\alpha_q$  and  $\beta\gamma$  subunits before Oxo-M treatment. There was no significant difference in the  $\tau$  values of step 1 (ON and OFF) between wild-type G $\alpha_q$  and G $\alpha_q$ (Q209L) (Fig. 4e). These results suggest that YM did not affect the interaction of G $\alpha_q$  protein with Oxo-M-activated hM3R but selectively inhibited the step 2

response by blocking the reaction of GDP release from the G $\alpha_q$  protein and the following GTP binding and separation of the heterotrimeric G $\alpha_q$  protein to G $\alpha_q$  and  $\beta\gamma$  subunits (Fig. 4f).

The molecular mechanism of the single-step FRET response under YM treatment was further studied in cells expressing hM3R-CFP plus G $\beta$ 1-YFP. Consistently, as shown in Fig. 4g, h, YM did not affect the interaction between hM3R-CFP and G $\beta$ 1-YFP by Oxo-M. Moreover, the

**Fig. 2 | Two-step activation kinetics of hM3R-YFP-CFP FRET correspond to hM3R-G<sub>q</sub> protein interaction and G<sub>α<sub>q</sub></sub> and G<sub>βγ</sub> dissociation, respectively.**

**a** Schematic of hM3R-CFP (hM3R-C), G<sub>β1</sub>-YFP (G<sub>β1</sub>-Y), and cognate G protein subunits at the plasma membrane. **b** Normalized FRET<sub>r</sub> in response to Oxo-M in cells intracellularly perfused with 0.1 mM GTP (left) or 1 mM GDPβS (right) through whole-cell configuration. Sampling frequency: 10 Hz. Yellow vertical lines indicate SEM. GTP, *n* = 8 (three cultures); GDPβS, *n* = 9 (three cultures). Percent of single step (% ON) in total FRET<sub>r</sub> response (**c**) and τ<sub>ON</sub> of onset of FRET<sub>r</sub> change (**d**). GTP, *n* = 8 (three cultures); GDPβS *n* = 9 (three cultures). Welch's *t* test (two-sided) and Student's *t* test (two-sided), respectively. **e** SNR of ΔFRET<sub>r</sub> in response to Oxo-M in cells expressing each FRET sensor. The cells were intracellularly perfused with 0.1 mM GTP except the fourth column (1 mM GDPβS). First and second columns, *n* = 7 (three cultures); third column, *n* = 8 (four cultures); fourth column, *n* = 9 (three cultures). Welch's *t* test (first-third columns), two-sided, \*\**p* = 0.0014; one-way ANOVA test with Tukey post hoc test (\*\**p* = 0.0003; second-third columns

\*\**p* = 0.0043, second-fourth columns \*\*\**p* = 0.0003, third-fourth columns *p* = 0.5728). **f** Schematic of wild-type hM3R, G<sub>α<sub>q</sub></sub>-CFP (G<sub>α<sub>q</sub></sub>-C), G<sub>β1</sub>-YFP, and Gy2 at the plasma membrane. GRK2 was co-expressed but not presented in the depiction. **g** Normalized FRET<sub>r</sub> in response to Oxo-M in cells intracellularly perfused with 0.1 mM GTP (left) or 1 mM GDPβS (right) through whole-cell configuration. Sampling frequency: 10 Hz. GTP, *n* = 6 (two cultures); GDPβS, *n* = 9 (three cultures). Percent of single step in total FRET<sub>r</sub> response (**h**) and τ<sub>ON</sub> of onset of FRET<sub>r</sub> change (**i**). GTP, *n* = 6 (two cultures); GDPβS, *n* = 9 (three cultures). Welch's *t* test (two-sided, \*\*\**p* = 0.0003). **j** SNR of ΔFRET<sub>r</sub> in response to Oxo-M application in cells expressing each FRET sensor. First and second columns, *n* = 7 (three cultures); third column, *n* = 6 (two cultures); fourth column, *n* = 9 (three cultures). Welch's *t* test (first-third columns), two-sided, \*\**p* = 0.0074; one-way ANOVA test with Tukey post hoc test (*p* = 0.1299; second-third columns *p* = 0.5800, second-fourth columns *p* = 0.1099, third-fourth columns *p* = 0.6022). Data are shown as mean ± SEM. ns not significant. Source data are provided as a Source Data file.

interaction between hM3R-CFP and G<sub>β1</sub>-YFP in cells expressing mutant G<sub>q</sub>(Q209L) was normal. We also examined the effects of YM in cells expressing G<sub>α<sub>q</sub></sub>-CFP plus G<sub>β1</sub>-YFP. In those cells, YM inhibited the activation of the G<sub>q</sub> protein and thus blocked the separation of G<sub>α<sub>q</sub></sub>-CFP and G<sub>β1</sub>-YFP (Fig. 4i, left). Then, after the removal of the YM, there was a slow FRET<sub>r</sub> decrease by the separation of G<sub>α<sub>q</sub></sub> and G<sub>βγ</sub> subunits. Interestingly, a minor but significant decrease in FRET<sub>r</sub> was detected after Oxo-M application even in the presence of YM, suggesting that the association of heterotrimeric G<sub>q</sub> protein with ligand-activated hM3R may result in the structural rearrangement between G<sub>α<sub>q</sub></sub> and G<sub>βγ</sub> subunits although they are still closely associated with each other. In cells expressing mutant G<sub>α<sub>q</sub></sub>(Q209L)-CFP plus G<sub>β1</sub>-YFP, there were no changes in FRET<sub>r</sub> after YM washout, supporting the idea that G<sub>α<sub>q</sub></sub>(Q209L)-CFP and G<sub>β1</sub>-YFP were already separated and not affected by either YM or receptor activation (Fig. 4i, j). We additionally examined whether this G<sub>α<sub>q</sub></sub>(Q209L)-CFP, which has no interaction with G<sub>βγ</sub>, is normally anchored to the plasma membrane. The confocal microscopy imaging showed no difference in the fluorescent expression level of G<sub>α<sub>q</sub></sub>-CFP and G<sub>β1</sub>-YFP in the plasma membrane or cytosol depending on whether G<sub>α<sub>q</sub></sub> was mutated in the resting state (Supplementary Fig. 15a–f). Moreover, in both conditions, receptor activation did not change those signal levels (Supplementary Fig. 15a–d). However, there was a difference in the regulation of PIP<sub>2</sub> levels. Oxo-M hydrolyzed the PIP<sub>2</sub> and increased the intracellular level of RFP-PH in cells expressing wild-type G<sub>α<sub>q</sub></sub>-CFP and G<sub>β1</sub>-YFP (Supplementary Fig. 15a). In contrast, in cells expressing mutant G<sub>α<sub>q</sub></sub>(Q209L)-CFP and G<sub>β1</sub>-YFP, the cytosolic level of RFP-PH was already elevated regardless of receptor activation, confirming that G<sub>α<sub>q</sub></sub>(Q209L)-CFP can activate PLC even without receptor stimulation (Supplementary Fig. 15b).

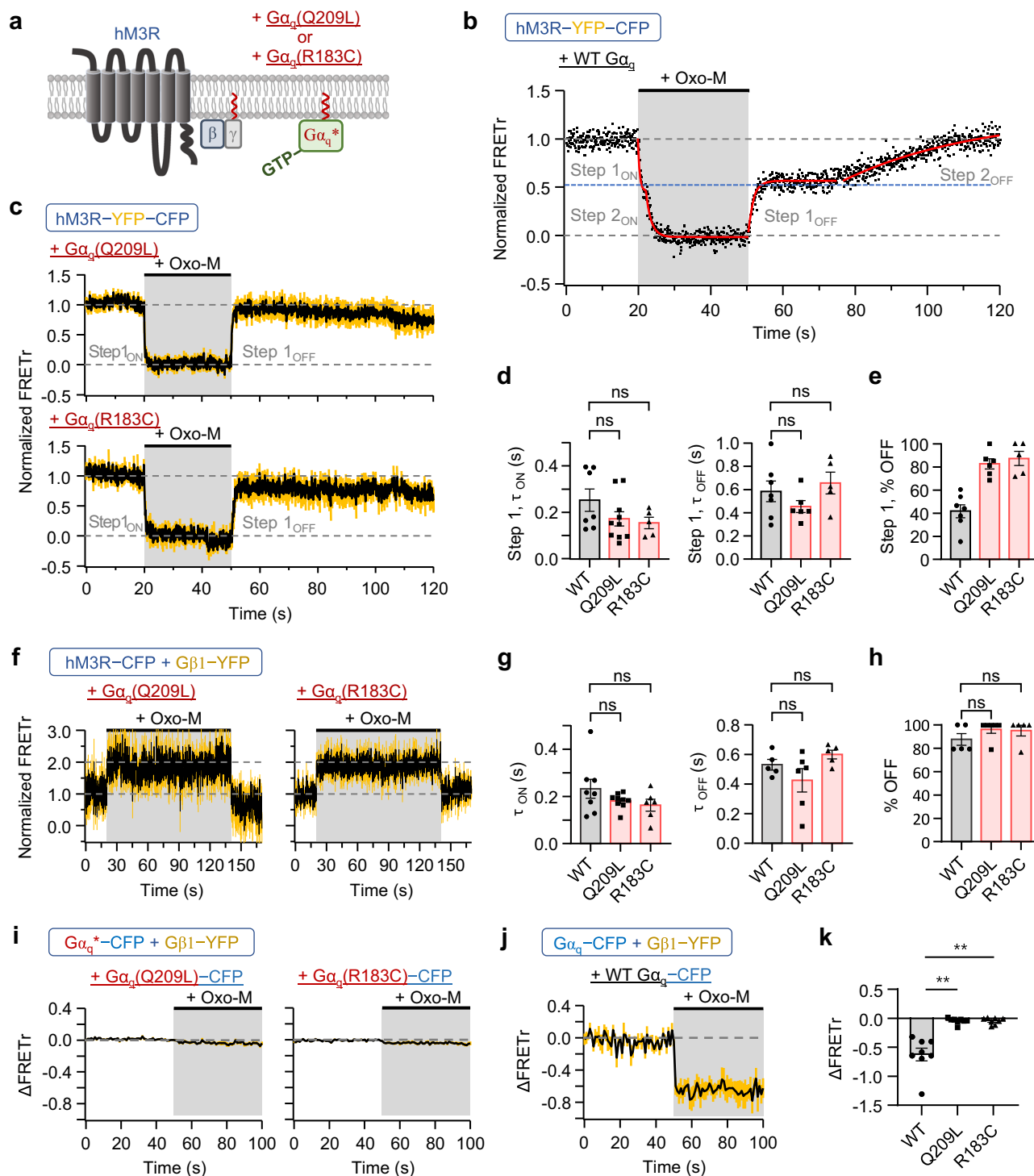
**Two-step structural change in hM3R-YFP-CFP depends on G protein coupling**

Existing fluorescence-based M3 sensors commonly show a single-step FRET change, which represents the conformational activation of a receptor by agonist binding<sup>37,38,45–47</sup>. To examine whether the two-step FRET signal observed in hM3R-YFP-CFP, especially in step 1, involves receptor activation in addition to G<sub>q</sub>-protein coupling, we applied a class A GPCR mutation strategy that blocks G<sub>α</sub> binding to our hM3R-YFP-CFP construct without impairing receptor activation by the ligand<sup>48</sup>. The three amino acid residues at positions 3x46 in TM3, 6x37 in TM6, and 7x53 in TM7 (notation represents the GPCRdb numbering scheme<sup>49</sup> from GPCRdb [<http://www.gpcrdb.org>]<sup>50</sup>) are conserved in all class A GPCRs and important for the cytosolic release of 6x37, which comes in contact with a universally conserved leucine residue (position G.H5.25; notation taken from “The Common G Protein Numbering Scheme”<sup>51</sup>) of the G<sub>α</sub> subunit<sup>48</sup> upon activation. This leucine residue plays a pivotal role in the coupling of G<sub>α</sub> to GPCRs<sup>52</sup>. Through modeling of the 3D structure of M3R(3A) using both I-TASSER and SWISS-Model, we confirmed that the allosteric effect of alanine substitution

on the structure or operation of the receptor's agonist-binding sites<sup>53</sup> was insignificant<sup>48</sup> (Fig. 5a, left; Supplementary Fig. 16, left). To block the G<sub>q</sub> protein coupling of hM3R-YFP-CFP, we substituted the corresponding I162 (3x46), L493 (6x37), and Y544 (7x53) residues with alanine in the construct. We found that the mutant hM3R(3A)-YFP-CFP was normally expressed in the cell membrane, but PIP<sub>2</sub> was not hydrolyzed even after the receptor was activated by Oxo-M or Ach (Fig. 5b, c). Next, the FRET signal of hM3R(3A)-YFP-CFP was measured after the treatment with these two agonists. Unlike the wild-type hM3R-YFP-CFP, hM3R(3A)-YFP-CFP displayed no considerable FRET<sub>r</sub> changes (Fig. 5d, e). These results suggested that hM3R(3A)-YFP-CFP could not interact with the heterotrimeric G<sub>q</sub> protein; this result was consistent with previous findings on class A receptors<sup>48</sup>. We also conducted FRET experiments between hM3R(3A)-CFP and G<sub>β1</sub>-YFP. As expected, the 3A mutant receptor did not interact with G<sub>q</sub> proteins (Fig. 5f, g). Therefore, the FRET<sub>r</sub> signal of hM3R-YFP-CFP represents the conformational changes induced by G<sub>q</sub> protein coupling but not the structural activation of the receptor by ligand binding. To convincingly show that the step 1 of hM3R-YFP-CFP is caused by G<sub>q</sub> coupling and not by ligand binding-induced conformational changes, we also examined the activity of single-leucine mutant (3x50) M3R which has been shown to block G<sub>q</sub> signaling but still undergo ligand-induced conformational rearrangement and arrestin-coupling<sup>54</sup>. As a result, the mutant hM3R(R166L<sup>3x50</sup>)-YFP-CFP displayed no considerable PIP<sub>2</sub> hydrolysis and FRET<sub>r</sub> changes (Supplementary Fig. 17).

**Independent binding of G<sub>βγ</sub> to hM3R may require the coupling of G<sub>α<sub>q</sub></sub>-GTP to the receptor**

To further understand the coupling mechanism between hM3R and separated G<sub>βγ</sub> subunits, we examined the independent G<sub>βγ</sub> interaction with the mutant hM3R(3A). First, consistent with the results shown in Fig. 5f, g, the findings indicated that coupling was normal between the wild-type hM3R-YFP and G<sub>α<sub>q</sub></sub>-CFP but completely abolished between hM3R(3A)-YFP and G<sub>α<sub>q</sub></sub>-CFP (Fig. 6a, b). Similarly, G<sub>α<sub>q</sub></sub>(Q209L)-CFP coupled with the wild-type hM3R-YFP but not with hM3R(3A)-YFP (Fig. 6c, d). Interestingly, the maximum change in the relative FRET<sub>r</sub> signal was strongly reduced in cells expressing the wild-type hM3R-YFP plus G<sub>α<sub>q</sub></sub>(Q209L)-CFP compared with that in cells expressing the wild-type hM3R-YFP plus wild-type G<sub>α<sub>q</sub></sub>-CFP (WT G<sub>α<sub>q</sub></sub>-CFP: 0.030 ± 0.002; G<sub>α<sub>q</sub></sub>(Q209L)-CFP: 0.014 ± 0.003, \*\*\**p* = 0.0006; Fig. 6b, d). Next, we measured the FRET<sub>r</sub> signal in cells expressing hM3R(3A)-YFP-CFP, G<sub>α<sub>q</sub></sub>(Q209L), and the rest of the wild-type cognate G protein subunits. Unlike the responses of the wild-type hM3R-YFP-CFP (Fig. 6e, f, left), the FRET<sub>r</sub> signal did not decrease in hM3R(3A)-YFP-CFP (Fig. 6e, f, right). Finally, we examined the direct binding of the separated G<sub>βγ</sub> to hM3R in cells co-transfected with G<sub>α<sub>q</sub></sub>(Q209L). As shown in Fig. 6g, h, FRET<sub>r</sub> did not change in cells expressing the mutant hM3R(3A)-CFP. These results suggest that the separated G<sub>βγ</sub> subunits could bind only to receptors coupled with G<sub>α<sub>q</sub></sub>-GTP.



### Sustained assembly of hM3R, Gα<sub>q</sub>, and PLCβ<sub>1</sub> during receptor activation

To determine the operating role of Gα<sub>q</sub> in the regulation of hM3R conformation, we performed FRETTr experiments in cells transfected with hM3R-YFP, Gα<sub>q</sub>-CFP, and cognate G protein subunits. The receptor activation upon Oxo-M application showed a single-step FRETTr increase, suggesting the interaction of hM3R-YFP with Gα<sub>q</sub>-CFP (Fig. 7a, d). Interestingly, the increased FRETTr signal was maintained during the Oxo-M treatment. After Oxo-M removal, the FRETTr signal returned to baseline through two-step kinetics with almost equal proportions (Fig. 7a, f). To investigate this two-step recovery, we first conducted the same FRETTr experiments in the presence of YM

(Supplementary Fig. 18a). There was a single-step increase in FRETTr like without YM, with a τ of around 0.2 s (Fig. 7e; Supplementary Fig. 18f, left). This was very similar to the step 1 τ (-0.21 s) of hM3R-YFP-CFP, confirming that the fast step 1<sub>ON</sub> response of hM3R-YFP-CFP is mediated by the coupling of hM3R with heterotrimeric inactive G<sub>q</sub> protein. Importantly, in the presence of YM, there was only a single-step FRETTr recovery (Supplementary Fig. 18a), with the time constant similar to the step 1<sub>OFF</sub> of hM3R-YFP plus Gα<sub>q</sub>-CFP (Fig. 7g) and step 1<sub>OFF</sub> of hM3R-YFP-CFP (Supplementary Fig. 8a, d). Based on these results, we can speculate that the two-step recovery of FRETTr in cells with hM3R-YFP and Gα<sub>q</sub>-CFP can be defined as the step 1<sub>OFF</sub> and step 2<sub>OFF</sub> responses in hM3R-YFP-CFP, where step 1<sub>OFF</sub> may indicate the release

**Fig. 3 | hM3R-YFP-CFP shows only step  $I_{ON}$  and  $I_{OFF}$  in presence of constitutively active  $G_{\alpha_q}$  proteins.** **a** Schematic of wild-type (WT) hM3R with the constitutively active mutant form of  $G_{\alpha_q}$ ,  $G_{\alpha_q}(Q209L)$  or  $G_{\alpha_q}(R183C)$  at the plasma membrane. **b** Normalized FRET $\tau$  signal in response to Oxo-M in cell expressing hM3R-YFP-CFP and WT  $G_q$  proteins ( $G_{\alpha_q}$ ,  $G\beta_1$ , and  $G\gamma_2$ ). Sampling frequency: 10 Hz. Red lines are single-exponential fits for step  $I_{ON}$ , step  $I_{OFF}$ , and step  $I_{OFF}$ . **c** Normalized FRET $\tau$  in cells expressing hM3R-YFP-CFP, mutant  $G_{\alpha_q}$  (Q209L or R183C), and cognate G protein subunits. Sampling frequency: 10 Hz. Yellow vertical lines indicate SEM. Q209L,  $n = 6$  (two cultures); R183C,  $n = 5$  (two cultures). **d**  $\tau$  for step  $I_{ON}$  and  $I_{OFF}$ . For  $\tau_{ON}$ , WT,  $n = 7$  (three cultures); Q209L,  $n = 10$  (two cultures); R183C,  $n = 5$  (two cultures). One-way ANOVA test ( $p = 0.1972$ ) with Tukey post hoc test (WT-Q209L,  $p = 0.2688$ ; WT-R183C,  $p = 0.2497$ ; Q209L-R183C,  $p = 0.9445$ ). For  $\tau_{OFF}$ , WT,  $n = 7$  (three cultures); Q209L,  $n = 6$  (two cultures); R183C,  $n = 5$  (two cultures). One-way ANOVA test ( $p = 0.2522$ ) with Tukey post hoc test (WT-Q209L,  $p = 0.4861$ ; WT-R183C,  $p = 0.8014$ ; Q209L-R183C,  $p = 0.2390$ ). **e** FRET $\tau$  recovery (% OFF) of step 1. WT,  $n = 7$  (three cultures); Q209L,  $n = 6$  (two cultures); R183C,  $n = 5$  (two cultures). **f** Normalized FRET $\tau$  signals in cells expressing hM3R-CFP,  $G\beta_1$ -YFP, mutant  $G_{\alpha_q}$  (Q209L or R183C), and  $G\gamma_2$ . Sampling frequency: 10 Hz. Q209L,  $n = 6$

(two cultures); R183C,  $n = 5$  (two cultures). **g**  $\tau$  of onset and offset of FRET $\tau$  changes by Oxo-M treatment. For  $\tau_{ON}$ , WT,  $n = 8$  (two cultures); Q209L,  $n = 9$  (two cultures); R183C,  $n = 6$  (two cultures). One-way ANOVA test ( $p = 0.2202$ ) with Tukey post hoc test (WT-Q209L,  $p = 0.3672$ ; WT-R183C,  $p = 0.2369$ ; Q209L-R183C,  $p = 0.8971$ ). For  $\tau_{OFF}$ , WT,  $n = 5$  (two cultures); Q209L,  $n = 6$  (two cultures); R183C,  $n = 5$  (two cultures). One-way ANOVA test ( $p = 0.1270$ ) with Tukey post hoc test (WT-Q209L,  $p = 0.4149$ ; WT-R183C,  $p = 0.6929$ ; Q209L-R183C,  $p = 0.1134$ ). **h** FRET $\tau$  recovery (% OFF). WT,  $n = 5$  (two cultures); Q209L,  $n = 6$  (two cultures); R183C,  $n = 5$  (two cultures). One-way ANOVA test ( $p = 0.3380$ ) with Tukey post hoc test (WT-Q209L,  $p = 0.3479$ ; WT-R183C,  $p = 0.4737$ ; Q209L-R183C,  $p = 0.9800$ ).  $\Delta$ FRET $\tau$  signals in cells expressing WT hM3R,  $G_{\alpha_q}$ -CFP (Q209L or R183C (**i**), WT (**j**)),  $G\beta_1$ -YFP,  $G\gamma_2$ , and GRK2. Sampling frequency: 1 Hz. Yellow vertical lines indicate SEM. Q209L,  $n = 8$  (two cultures); R183C,  $n = 8$  (two cultures); WT  $G_{\alpha_q}$ ,  $n = 8$  (two cultures). **k** Average  $\Delta$ FRET $\tau$  during Oxo-M application in experiments (**i**) and (**j**). Welch's ANOVA test ( $p = 0.0008$ ) with Games-Howell post hoc test (WT-Q209L,  $**p = 0.0025$ ; WT-R183C,  $**p = 0.0026$ ; Q209L-R183C,  $p = 0.9925$ ). Data are shown as mean  $\pm$  SEM. ns not significant. Source data are provided as a Source Data file.

of  $G\beta\gamma$  subunit from hM3R after the uncoupling of Oxo-M from hM3R and step  $I_{OFF}$  could be a result of the dissociation of  $G_{\alpha_q}$ -CFP from hM3R-YFP after the hydrolysis of GTP to GDP by the GTPase activity of  $G_{\alpha_q}$  (Fig. 7a). This speculation was further tested using the mutant  $G_{\alpha_q}(Q209L)$ . As shown in Fig. 7b, f, no significant step  $I_{OFF}$  response was observed after the Oxo-M washout. Consistently, the step  $I_{ON}$  response decreased in cells expressing  $G_{\alpha_q}(Q209L)$  because of the independent binding of  $G\beta\gamma$  to the receptor (Fig. 7c). However, the kinetics of step  $I_{ON}$  and  $I_{OFF}$  remained unchanged (Fig. 7e, g). These results further supported that the slow step  $I_{OFF}$  in the FRET $\tau$  response of hM3R-YFP plus  $G_{\alpha_q}$ -CFP was due to the slow dissociation of  $G_{\alpha_q}$ -CFP from hM3R-YFP. Through confocal microscopy imaging, we further confirmed that the cells transfected with hM3R-YFP,  $G_{\alpha_q}$ -CFP, and cognate G protein subunits also possessed a normal signaling cascade to PLC $\beta$  activation and PIP $_2$  hydrolysis by receptor activation (Supplementary Fig. 19a). In addition, the hM3R signaling to PLC $\beta$  activation was sustained until washout of the agonist (Supplementary Fig. 19b).

To investigate the interaction of activated  $G_{\alpha_q}$ -GTP with its effector PLC $\beta$ , we performed FRET $\tau$  experiments in cells transfected with hM3R,  $G_{\alpha_q}$ -CFP, YFP-PLC $\beta_1$ , and cognate G protein subunits. The receptor activation upon Oxo-M application showed a single-step FRET $\tau$  increase that was stronger but slower than that of hM3R-YFP and  $G_{\alpha_q}$ -CFP, suggesting that the coupling between hM3R and  $G_{\alpha_q}$  is completed faster than the complex formation of  $G_{\alpha_q}$  and PLC $\beta_1$  (Fig. 7h, i). Surprisingly, the increased FRET $\tau$  signal between  $G_{\alpha_q}$ -CFP and YFP-PLC $\beta_1$  was also maintained during the activation of the receptor (Fig. 7h). When checking the deactivation process in  $G_{\alpha_q}$ -CFP plus YFP-PLC $\beta_1$ , a single-step decrease was measured (Fig. 7h, j). The kinetics of this single-step deactivation was found to be slower than the step  $I_{OFF}$  reaction of hM3R-YFP plus  $G_{\alpha_q}$ -CFP (Fig. 7g left) or hM3R-YFP-CFP (Supplementary Fig. 8a, d) but faster than the step  $I_{OFF}$  reaction of hM3R-YFP plus  $G_{\alpha_q}$ -CFP (Fig. 7g, right) or hM3R-YFP-CFP (Supplementary Fig. 8a, e).

Considering the stable interaction between active hM3R and  $G_{\alpha_q}$ -GTP (Fig. 7a), the results suggested that hM3R,  $G_{\alpha_q}$ , and PLC $\beta_1$  formed a stable heterotrimeric complex during receptor activation. To test this possibility, we examined the direct interaction between hM3R-CFP and YFP-PLC $\beta_1$ . As shown in Fig. 7k, Oxo-M strongly increased the FRET $\tau$  signal in cells expressing the two probes, supporting the conclusion that a stable complex formed between M3R and PLC $\beta_1$  upon receptor activation. The analysis of the FRET $\tau$  signals revealed two-step responses during activation and deactivation (Fig. 7l, m, right). Interestingly, the kinetics of the fast steps  $I_{ON}$  and  $I_{OFF}$  was similar to that of receptor activation (Fig. 7l, m, left). The kinetics of step  $I_{OFF}$  was close to that of the step  $I_{OFF}$  of hM3R-YFP and  $G_{\alpha_q}$ -CFP (Fig. 7g, right),

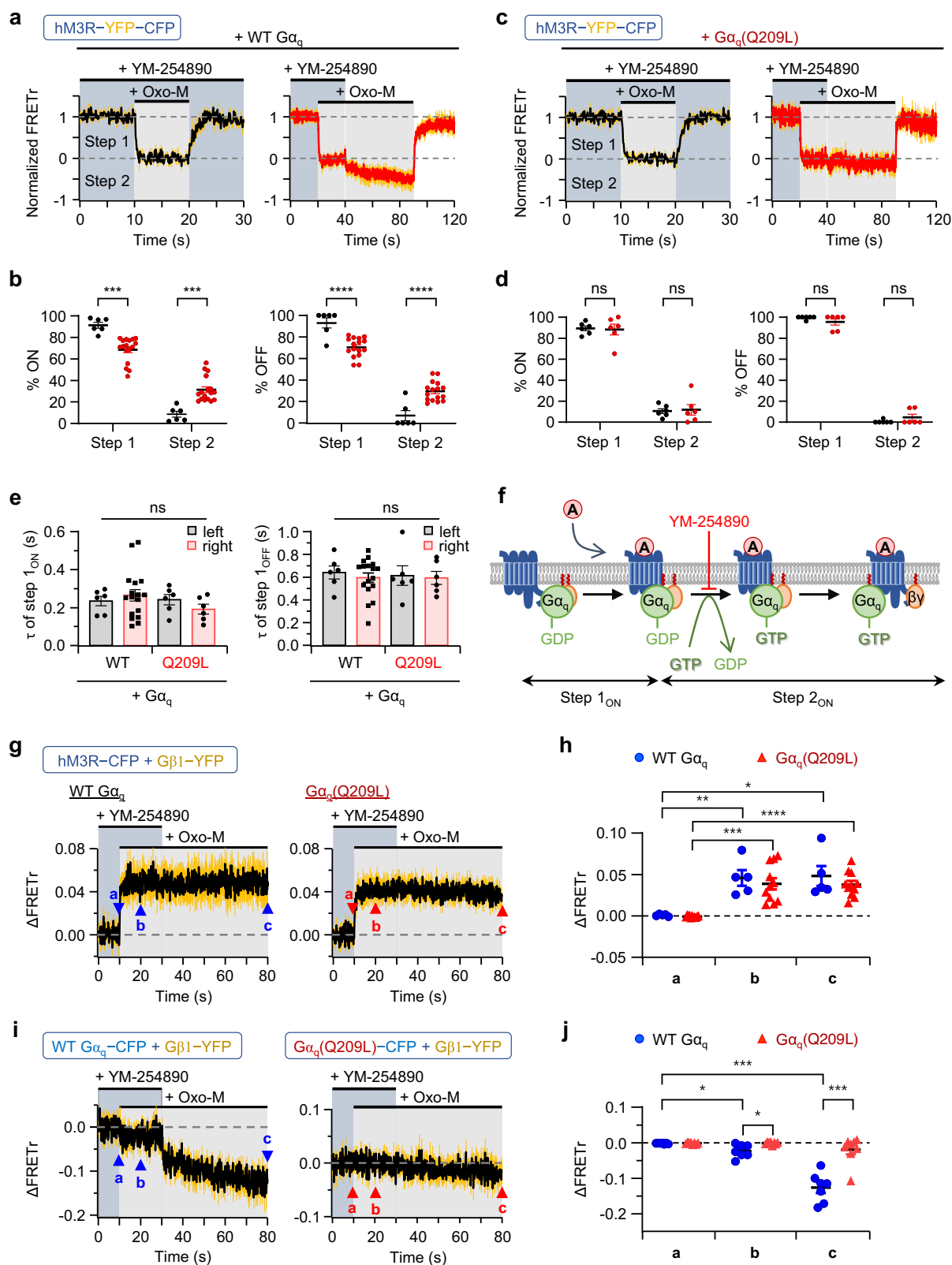
suggesting that PLC $\beta_1$  might dissociate from hM3R when  $G_{\alpha_q}$  left the receptor. Together, the results demonstrate that PLC $\beta_1$  is released from  $G_{\alpha_q}$ -GTP more slowly than the step  $I_{OFF}$  reaction and that this release ends before the completion of the step  $I_{OFF}$  reaction (Fig. 8). Finally, to check the function of YM, we conducted the same FRET $\tau$  experiments with  $G_{\alpha_q}$ -CFP plus YFP-PLC $\beta_1$  in the presence of YM (Supplementary Fig. 18b–f). There was no FRET $\tau$  change by receptor activation, indicating that YM successfully inhibited  $G_q$  activation by blocking the GDP release from  $G_{\alpha_q}$ . The results further confirmed that the inactive  $G_q$  protein cannot interact with PLC $\beta_1$ .

## Discussion

Various GPCR studies using FRET probes, bioluminescence resonance energy transfer (BRET) probes, or cpGFP (circularly permuted green fluorescent protein) have been conducted to observe the intramolecular conformational change of receptors by ligand binding<sup>36–38,46,55–61</sup>. However, to observe the GPCR signaling pathways after receptor activation, additional experiments<sup>36,38,62,63</sup> are required utilizing new photo probes corresponding to each pathway step. In those step-by-step experiments for the signaling cascades, the continuity of the entire structural deformation of GPCR is inevitably damaged. In this study, we overcame these limitations by constructing a M3R FRET sensor hM3R-YFP-CFP. Using the construct, we discovered that the structure of hM3R reversibly changed through a multistep process according to the activation cycle of the  $G_q$  protein. In addition, the FRET results among M3R,  $G_{\alpha_q}$ , and PLC $\beta$  suggested that the ligand-activated M3R formed a sustained heterotrimeric complex with  $G_{\alpha_q}$  and PLC $\beta$ .

Here, we reported the two-step activation and deactivation of M3R. All existing fluorescence-based M3 sensors commonly displayed receptor activation through a single-step change in fluorescent signals. In previous studies, the activation of a receptor generally corresponds to the conversion of the M3R structure from an inactive state to an active one after agonist binding and not to the structural changes induced by G protein coupling. However, hM3R-YFP-CFP exhibited completely different properties from the existing sensors in that it detected G protein coupling after the activation stage and thus released the activation cycle of the G protein as a two-step FRET signal. This finding was further confirmed by the experiments involving the receptors with mutated  $G\alpha$ -binding sites without the impaired activation of the receptor<sup>48</sup>. The distinction in the target response of our receptor sensor might be attributed to the differences in receptor construction methods. For example, a fluorescence arsenical hairpin binder (FLASH)-based M3 FRET sensor<sup>37,38</sup> shows normal downstream signaling similar to our hM3R-YFP-CFP but only detects the receptor activation through the FRET response, and the direction of response is





increase that is opposite to ours. These differences might be due to the location and size of the inserted amino-acid motif CCPGCC, where the amino-acid residues from 271 and 465 (193 amino acids) of ICL3 were replaced with CCPGCC (7 amino acids); in our construct, the residues between 270 and 485 (214 amino acids) were replaced with *SacII*-EYFP-*AgeI* (243 amino acids) in ICL3. In addition, the sensor required an additional binding of FIAsh to the inserted CCPGCC. Thus,

such differences possibly led to the differential positioning of acceptor fluorescence (FIAsh or EYFP) relative to CFP between these two FRET sensors; eventually, the stage of signaling pathways and the direction of the FRET response varied. Similarly, GACH2.0 (ACh2.0)<sup>46</sup> and GRAB<sub>ACh3.0</sub> (ACh3.0)<sup>45</sup> were constructed by inserting cpGFP into ICL3; when the receptor becomes activated, cpGFP transforms into an intact GFP structure and emits fluorescence. Unlike hM3R-YFP-CFP, this

**Fig. 4 | YM-254890 (YM) blocks the step 2 stage of hM3R-YFP-CFP activation.** In figures (a–e), cells were transfected with hM3R-YFP-CFP,  $G\alpha_q$  (wild-type (WT) or Q209L), and cognate G protein subunits. Time courses of normalized FRET signals in response to Oxo-M in cells expressing WT  $G\alpha_q$  (a) or mutant  $G\alpha_q$  (Q209L) (c) during continuous (left black trace,  $n = 6$ , two cultures, respectively) or temporary (right red trace,  $n = 17$ , three cultures for WT;  $n = 6$ , two cultures for  $G\alpha_q$  (Q209L)) medication of YM. Sampling frequency: 10 Hz. Yellow vertical lines indicate SEM of each time point. **b** Percent distribution of each step during activation (ON) or deactivation (OFF) of hM3R-YFP-CFP in figure (a). Student's *t* test (% ON, two-sided,  $***p = 0.0002$ ; % OFF, two-sided,  $****p < 0.0001$ ). **d** Percent distribution of each step during hM3R-YFP-CFP activation (ON) or deactivation (OFF) in figure (c). Student's *t* test (% ON, two-sided) and Welch's *t* test (% OFF, two-sided). **e**  $\tau$  of step  $I_{ON}$  and step  $I_{OFF}$  shown in figures (a) and (c). The values of step 2 were not compared. Two-way ANOVA test with Tukey post hoc test. **f** Schematic showing the action step of YM.

**g** Time course of  $\Delta$ FRET signals in response to Oxo-M in cells expressing hM3R-CFP,  $G\beta_1$ -YFP, Gy2, and WT  $G\alpha_q$  (left,  $n = 5$ , two cultures) or mutant  $G\alpha_q$  (Q209L) (right,  $n = 11$ , three cultures) during temporary medication of YM. Sampling frequency: 10 Hz. **h** Average of  $\Delta$ FRET at each marked time period (a: 0.0–9.9 s; b: 10–20 s; c: 70–80 s) in figure (g). Paired *t* test (two-sided). WT  $G\alpha_q$  (a,  $b^{**}p = 0.0077$ ; a–c  $*p = 0.0163$ ),  $G\alpha_q$  (Q209L) (a,  $b^{***}p = 0.0002$ ; a–c  $****p < 0.0001$ ). **i** Time course of  $\Delta$ FRET signals in response to Oxo-M in cells expressing hM3R,  $G\beta_1$ -YFP, Gy2, GRK2, and WT  $G\alpha_q$ -CFP (left,  $n = 7$ , two cultures) or mutant  $G\alpha_q$  (Q209L)-CFP (right,  $n = 7$ , two cultures) during temporary medication of YM. **j** Average of  $\Delta$ FRET at each marked time period in (i). Paired *t* test (two-sided) within WT  $G\alpha_q$  (a–b  $*p = 0.0176$ ; a–c  $***p = 0.0002$ ), and Welch's *t* test (two-sided) between WT  $G\alpha_q$  and  $G\alpha_q$  (Q209L) at each time point (b  $*p = 0.0197$ ; c  $***p = 0.0002$ ). Data are shown as mean  $\pm$  SEM. ns not significant. Source data are provided as a Source Data file.

sensor is a dead form of downstream signaling and therefore can only detect receptor activation. This difference is also likely due to the locations of the inserted cpGFP instead of YFP. For ACh2.0, the residues between amino acids 253 and 493 (239 amino acids) of ICL3 were replaced with linker-cpGFP-linker (301 amino acids); for ACh3.0, the residues between amino acids 259 and 491 (231 amino acids) of ICL3 were replaced with linker-cpGFP-linker (246 amino acids). The ICL2 and ICL3 parts of GPCRs have conserved amino acids, which are essential for recognizing a certain type of G protein<sup>24,64</sup>. However, these amino acids were lost during cpGFP insertion; this loss likely caused these cpGFP-based sensors to become the dead form of downstream signaling.

Using hM3R-YFP-CFP, we demonstrated that a single-receptor FRET probe can reveal the multistep intramolecular conformational changes of a receptor during the coupled G protein cycle. We confirmed that, in the activation process, the association of ligand-activated hM3R with the inactive  $G_q$  protein displayed the fast step 1 FRET signal and the following dissociation of  $G\alpha_q$  and  $G\beta\gamma$  subunits under receptor coupling was responsible for the slower step 2 FRET signal (Fig. 8). We could not obtain any independent FRET change by ligand binding itself in hM3R-YFP-CFP even at a high frequency resolution (100 Hz) and fast solution exchange system ( $\sim 20$  ms). Previous studies have shown that ligand–M3R coupling is completed within 100 ms<sup>37,62</sup>, thus it is possible that the ligand binding to the external surface of our hM3R FRET construct generates relatively insignificant FRET change.

In our disease model studies using the constitutively active  $G\alpha_q$  (Q209L or R183C) forms, there was a single fast step of FRET change in hM3R-YFP-CFP alone and in hM3R-CFP plus  $G\beta_1$ -YFP. Since the  $G\beta\gamma$  subunits exist independently in resting cells after decoupling from the constitutively active  $G\alpha_q$  (Q209L or R183C), the results indicate that the ligand-activated hM3R can associate with the separated  $G\beta\gamma$  subunits. In addition, the hM3R- $G\beta\gamma$  coupling remains unchanged during the YM application, confirming that the fast step 1 FRET signal of hM3R-YFP-CFP in the presence of  $G\alpha_q$  (Q209L or R183C) is mostly mediated by the intermolecular interaction with the  $G\beta\gamma$  subunit. We also found that agonist binding to hM3R itself changes the interaction between  $G\alpha_q$  and  $G\beta\gamma$  subunits before dissociation. As shown in Fig. 4i, j, even in the presence of the GDP release inhibitor YM, there was a minor but significant FRET decrease between  $G\alpha_q$  and  $G\beta\gamma$  subunits after Oxo-M application. These initial structural changes between  $G\alpha_q$  and  $G\beta\gamma$  subunits upon binding to ligand-activated hM3R may be important for GDP release from the inactive  $G\alpha_q$  and subsequent GTP binding.

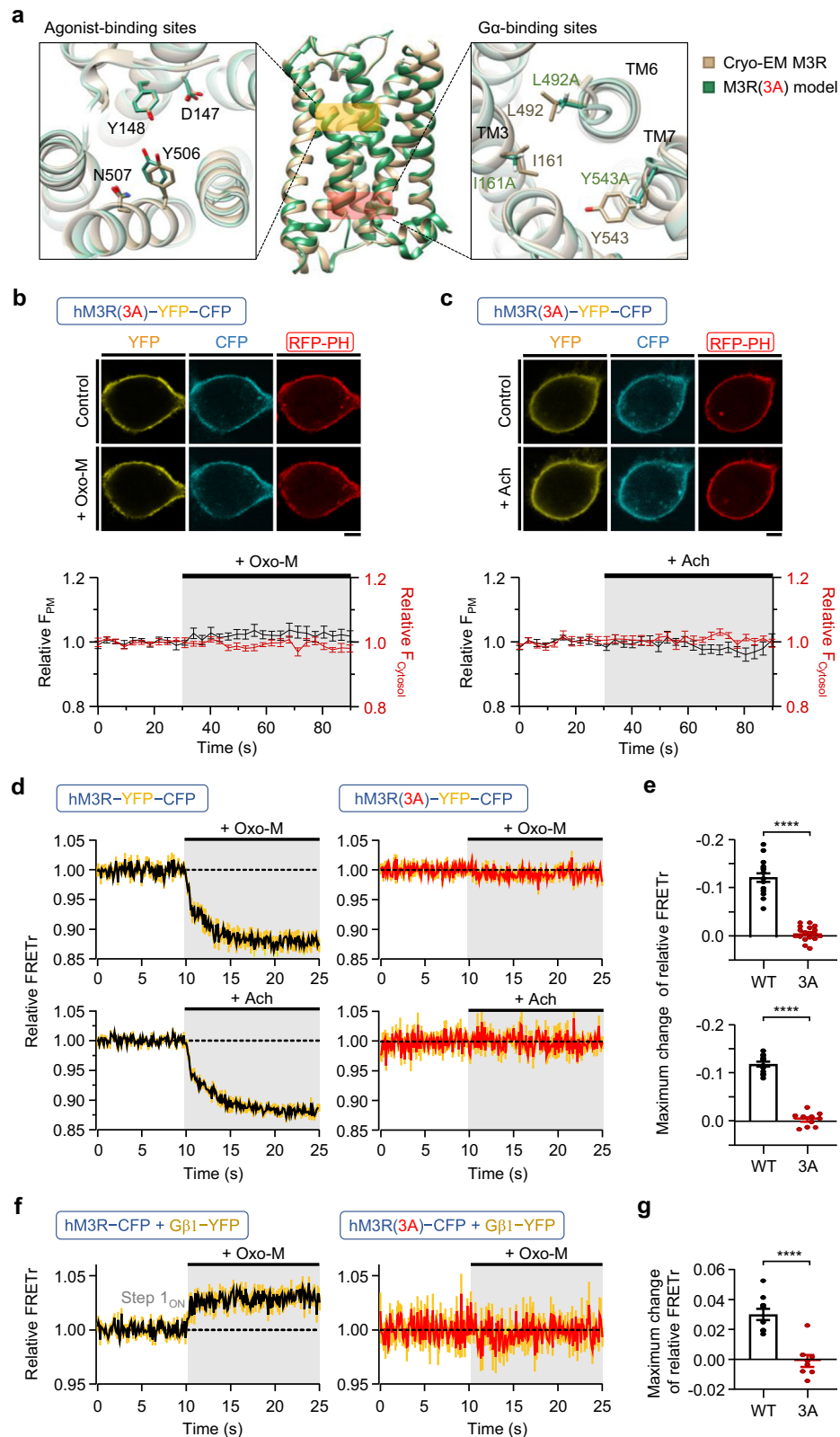
We confirmed that the loss of G protein coupling ability in the triple-alanine mutant (3x46/6x37/7x53) vasopressin V2 receptor<sup>48</sup> can be reproduced in M3R, which is the same class A GPCR. By constructing hM3R(3A), we revealed that hM3R-YFP-CFP only detected the downstream signals related to the activation cycle of  $G_q$  protein but not the precedent receptor activation step by ligand binding. This was further confirmed by additional experiments using single-leucine mutant (3x50) M3R. Previous study reported that the mutant

M3R(R165L<sup>3x50</sup>) still had normal agonist-binding affinity and arrestin-dependent signaling pathways<sup>54</sup>. Nevertheless, our hM3R(R165L<sup>3x50</sup>)-YFP-CFP showed no significant  $PIP_2$  hydrolysis and FRET changes (Supplementary Fig. 17).

Another significant finding is the two-step deactivation of FRET in cells expressing hM3R-YFP and  $G\alpha_q$ -CFP after washout of the agonist. The fast step 1 and the subsequent slower step 2 recoveries seem to be due to the sequential interaction changes by the decoupling of the  $G\beta\gamma$  subunit from hM3R following agonist dissociation and the dissociation of  $G\alpha_q$ -CFP from hM3R after the slow dephosphorylation of GTP to GDP by GTPase activity, respectively. These results suggest that, in the recovery process from receptor activation,  $G\alpha_q$ -GTP alone can be coupled with the receptor during the step 2 period even in the absence of the  $G\beta\gamma$  subunit on the receptor.

Several studies related to the inactive-state preassembly of GPCRs and G proteins have been reported recently<sup>24,26–33</sup>. However, the results have been contradictory even when using the same M3R<sup>33,65</sup>. The discrepancy might be due to the fact that the studies could not directly probe the stability of the protein–protein complex<sup>5</sup>. In the present study, we showed that there was a significant FRET increase between hM3R-CFP and  $G\beta_1$ -YFP, indicating that the activated hM3R interacts with heterotrimeric  $G_q$  protein to form a tight complex. However, the FRET signal amplitudes and the SNR were much smaller compared to the step 1 responses of hM3R-YFP-CFP. Those weak FRET signals compared to noises can be caused by the preassembly of inactive hM3R with the  $G\beta\gamma$  subunit of  $G_q$  protein in the resting state, although the association is not as tight as the condition under receptor activation. Thus, we speculate that agonist binding to hM3R may reorganize the preassembled complex to a closer conformation between the two probes.

It has generally been accepted that the activated  $G\alpha$ -GTP subunit dissociates from the receptor to yield a  $G\alpha$ -GTP monomer–effector complex, while the separated  $G\beta\gamma$  subunit stays complexed with the receptor, which is now free to modulate other intracellular signaling molecules independently. However, some heterotrimeric  $G_i$  and  $G_s$  proteins maintain assembly with receptors in the early stage of activation<sup>30,32</sup>. Here, our study demonstrates that  $G\alpha_q$ -GTP does not leave hM3R after dissociation from  $\beta\gamma$  subunits, and it continuously activates the downstream PLC $\beta$  molecule after forming a complex with hM3R until washout of the agonist. Interestingly, in our study, the increased FRET signal between  $G\alpha_q$ -CFP and YFP-PLC $\beta_1$  or between hM3R-CFP and YFP-PLC $\beta_1$  was also maintained steadily during the hM3R activation. These results are consistent with the sustained  $PIP_2$  depletion in the plasma membrane during the hM3R activation by the agonist (Supplementary Fig. 19). Therefore, in line with the previous studies showing that G protein can form a constitutive complex with effectors<sup>66–70</sup>, our results suggest that hM3R,  $G\alpha_q$ , and PLC $\beta$  form a stable heterotrimeric complex together induced by the agonist and cause the steady  $PIP_2$  hydrolysis until washout of the agonist.



## Methods

### Constructs

In the plasmid (Addgene plasmid # 45547) encoding the human M3D receptor, two point mutations (C149Y and G239A) were created to generate wild-type human M3R (hM3R). This hM3R was appended to pcDNA 3, which includes cerulean, a variant of enhanced cyan fluorescent protein (ECFP), to generate hM3R-Cerulean. The restriction

enzyme *Eco*RI recognition site mediated this appendage between Leu590 at the C terminus of hM3R and Met1 at the N terminus of cerulean. The cerulean of this hM3R-Cerulean was substituted with enhanced yellow fluorescent protein (EYFP) to generate hM3R-EYFP. To create the intramolecular fluorescent probe hM3R-EYFP-Cerulean, EYFP replaced a segment between Ala270 and Lys485 in the third intracellular loop of hM3R-Cerulean. The recognition sites of

**Fig. 5 | hM3R(3A) is not able to bind G<sub>q</sub> protein.** **a** Comparison of cryo-EM M3R (PDB ID: 4DAJ)<sup>53</sup> and I-TASSER 3D predicted M3R(3A) on orthosteric agonist-binding sites (left) and G<sub>α</sub>-binding sites (right, 3x46 (I161), 6x37 (L492), 7x53 (Y543)). The yellow and red boxes in the middle panel indicate agonist- and G<sub>α</sub>-binding regions of M3R, respectively. Amino acid residues on binding sites are shown as a stick in tan (cryo-EM M3R) or green (M3R(3A) model). Top, representative confocal images of cells expressing red fluorescent protein-labeled pleckstrin homology domain of PLC $\delta_1$  (RFP-PH) and hM3R(3A)-YFP-CFP were obtained before (Control) and during 10  $\mu$ M Oxo-M (**b**) or Ach (**c**) application. Scale bar, 5  $\mu$ m. Bottom, time courses of relative fluorescence intensity of RFP-PH at plasma membrane (black trace, left axis) and cytosol (red trace, right axis) were measured in 10–11 cells from three independent experiments. Sampling frequency: 0.33 Hz. **d** Time course of relative FRETr in response to 15 s of 10  $\mu$ M Oxo-M (top) or

Ach (bottom) in cells expressing wild-type (WT) hM3R-YFP-CFP (left) or hM3R(3A)-YFP-CFP (right). Sampling frequency: 10 Hz. Oxo-M treated hM3R-YFP-CFP,  $n = 16$  (two cultures); Oxo-M treated hM3R(3A)-YFP-CFP,  $n = 18$  (two cultures); Ach treated hM3R-YFP-CFP,  $n = 12$  (three cultures); Ach treated hM3R(3A)-YFP-CFP,  $n = 10$  (two cultures). **e** Maximum change of relative FRETr in each cell of figure (**d**) by 10  $\mu$ M Oxo-M (top) or Ach (bottom) treatment. Welch's  $t$  test (top) (two-sided, \*\*\*\* $p < 0.0001$ ), and Student's  $t$  test (bottom) (two-sided, \*\*\*\* $p < 0.0001$ ). **f** Time course of relative FRETr in response to 15 s of Oxo-M in cells expressing G $\alpha_q$ , G $\beta_1$ -YFP, G $\gamma_2$ , and hM3R-CFP (left,  $n = 10$ , two cultures) or hM3R(3A)-CFP (right,  $n = 8$ , three cultures). Sampling frequency: 10 Hz. Yellow vertical lines indicate SEM. **g** Maximum change of relative FRETr in each cell of (**f**) by Oxo-M treatment. Student's  $t$  test (two-sided, \*\*\*\* $p < 0.0001$ ). Data are shown as mean  $\pm$  SEM, with error bars indicating SEM. Source data are provided as a Source Data file.

restriction enzymes *Sac*II and *Age*I mediated this replacement. Three amino-acid point mutations (I162A, L493A and Y544A) of these hM3R-Cerulean, hM3R-EYFP, and hM3R-EYFP-Cerulean were created to generate hM3R(3A)-Cerulean, hM3R(3A)-EYFP, and hM3R(3A)-EYFP-Cerulean. One amino-acid point mutation (R166L) of the hM3R-EYFP-Cerulean was created to generate hM3R(R166L<sup>3x50</sup>)-EYFP-Cerulean. Point mutations of the existing human G $\alpha_q$ <sup>36</sup> and mouse G $\alpha_q$ -ECFP<sup>36,71,72</sup> were created to generate G $\alpha_q$ (Q209L), G $\alpha_q$ (R183C), G $\alpha_q$ (Q209L)-ECFP, and G $\alpha_q$ (R183C)-ECFP. All constructs were made using adaptations of the QuikChange (Agilent Technologies, Santa Clara, CA) mutagenesis protocol and restriction enzyme kits (Enzymomics, Daejeon, South Korea) and were verified by automated sequencing (Macrogen, Seoul, South Korea). The sequences of primers used for plasmid cloning are listed in Supplementary Table 1. Mouse MIR-YFP-CFP<sup>36</sup>, mouse G $\alpha_q$ -ECFP<sup>36,71,72</sup>, bovine G $\beta_1$ -EYFP<sup>36</sup>, rat EYFP-PLC $\beta_1$ <sup>36,72</sup>, and human pleckstrin homology (PH) domain probe RFP-PH(PLC $\delta_1$ )<sup>73</sup> were obtained from B. Hille (University of Washington School of Medicine, Seattle, WA). PH(PLC $\delta_1$ )-ECFP and PH(PLC $\delta_1$ )-EYFP<sup>36,74</sup> were obtained from K. Jalink (The Netherlands Cancer Institute, Amsterdam, Netherlands). Plasmids containing unlabeled mouse MIR, human G $\alpha_q$ , G $\beta_1$ , G $\gamma_2$ , and bovine GPCR kinase 2 (GRK2)<sup>36</sup> were obtained from B. Hille. Here, we refer to fluorophores simply as CFP or YFP regardless of whether regular or enhanced fluorescent proteins were used. We confirm that all used unique biological materials are readily available from the corresponding author.

### Cell culture

Human embryonic kidney tsA-201 cells (large T-antigen transformed HEK293 cells (HEK293T cells); RRID: CVCL\_2737) were a kind gift from Dr. Bertil Hille at University of Washington. The identity of this cell line has been authenticated by STR analysis and has recurrently tested negative for mycoplasma contamination using PCR (Cosmogenetech, Daejeon, South Korea). All experiments were performed on transiently transfected HEK293T cells. The 2-ml transfection medium contained 10  $\mu$ l of Lipofectamine-2000 and 0.2–0.8  $\mu$ g of each plasmid. In the G protein studies, for better membrane expression of any G protein subunit probe, cells were always transfected with three G protein subunits ( $\alpha$ ,  $\beta$ , and  $\gamma$ ) together. The next day, the cells were plated onto poly-L-lysine-coated #0 glass coverslip chips, and fluorescent cells were studied 36–48 h after transfection.

### Förster resonance energy transfer (FRET)

Our FRET system was described in our previous publications<sup>75–77</sup>. FRET between CFP and YFP was measured by a photomultiplier tube (PMT)-based photometry system (Till Photonics GmbH). Regular pulses of indigo light (426–450 nm) from a homemade LED-based monochromator excited the fluorescent proteins. Emission, which passed through a 40 $\times$ , NA 0.95 dry immersion objective lens (IX71; Olympus), was separated into short (460–500 nm) and long (520–550 nm) wavelengths by a dichroic mirror (505DCLP) and band-pass filters (D480-40 for short wavelengths and ET535-30 for long wavelengths;

Chroma Technology) and detected by two PMTs connected with an FDU-2 fluorescence detection unit (Till Photonics GmbH). Donor and acceptor signals obtained by photometry system were transferred to a data acquisition board (PCI-6221; National Instruments, or EPC-10; HEKA Elektronik). Timing control, signal acquisition, and real-time calculation of FRET ratio (FRETr) including background compensation, were performed using a homemade program or PatchMaster (HEKA Elektronik) that also controlled the monochromator through the data acquisition interface. To correct bleed-through of emission of CFP into the YFP detector, cells expressing only CFP were used to obtain the ratio of the detected signal in short and long wavelength emission channels<sup>36</sup>. The calculated ratio (cFactor = CFP/YFP = 0.45) was used to correct the raw YFP emission signal. The bleed-through of YFP light into the CFP detector was only 0.02 and was neglected. The FRETr was thus calculated as follows:

$$\text{FRETr} = (\text{YFP}_C - \text{cFactor} \times \text{CFP}_C) / \text{CFP}_C,$$

where YFP<sub>C</sub> is the signal from YFP excited as a result of FRET (YFP emission by CFP excitation), CFP<sub>C</sub> is the CFP emission detected by the short wavelength PMT, and YFP<sub>C</sub> is the YFP emission detected by the long wavelength PMT.

The whole-cell configuration of the patch-clamp method using an EPC-10 patch-clamp amplifier at room temperature was used to manipulate intracellular concentration of GTP, GDP $\beta$ S or GTP $\gamma$ S. Pipettes were pulled from glass micropipette capillaries (World Precision Instruments) using a Flaming/Brown micropipette puller (P-97; Sutter Instrument Co.). Pipette resistance was 1.3–3.0 M $\Omega$ , and series resistance was between 3.4 and 6.0 M $\Omega$  with 60% compensation. The pipette solution composition was described in Solutions and materials section. The holding potential in all experiments was –80 mV. The raw data were processed with Excel 2016 (Microsoft).

### Confocal imaging

HEK293T cells were imaged 2 d after transfection on poly-L-lysine-coated chips with a LSM 700 confocal microscope (Carl Zeiss) at room temperature. The images were scanned with a 40 $\times$  objective lens at 1024  $\times$  1024 or 512  $\times$  512 pixels using digital zoom on a cover glass-bottom dish filled with the external solution. Image processing and measurement of fluorescence intensity were carried out using Zeiss ZEN 2.3 SP1 software. To analyze relative fluorescence intensity, the fluorescence intensity of a region of interest (ROI) at each time point was divided by the average of points 30-s period before Oxo-M or Ach treatment. The half time of activation curve ( $T_{50}$ ) was calculated from sigmoidal curve fitting. All images were transferred from LSM4 to JPG format. The raw data were processed with Excel 2016 (Microsoft).

### Solutions and materials

Cells were subjected to a continuous slow bath flow of Ringer's solution. The fresh external Ringer's solution was supplied to the chamber by the valve-controlled gravity perfusion system VC3-4CLG from ALA

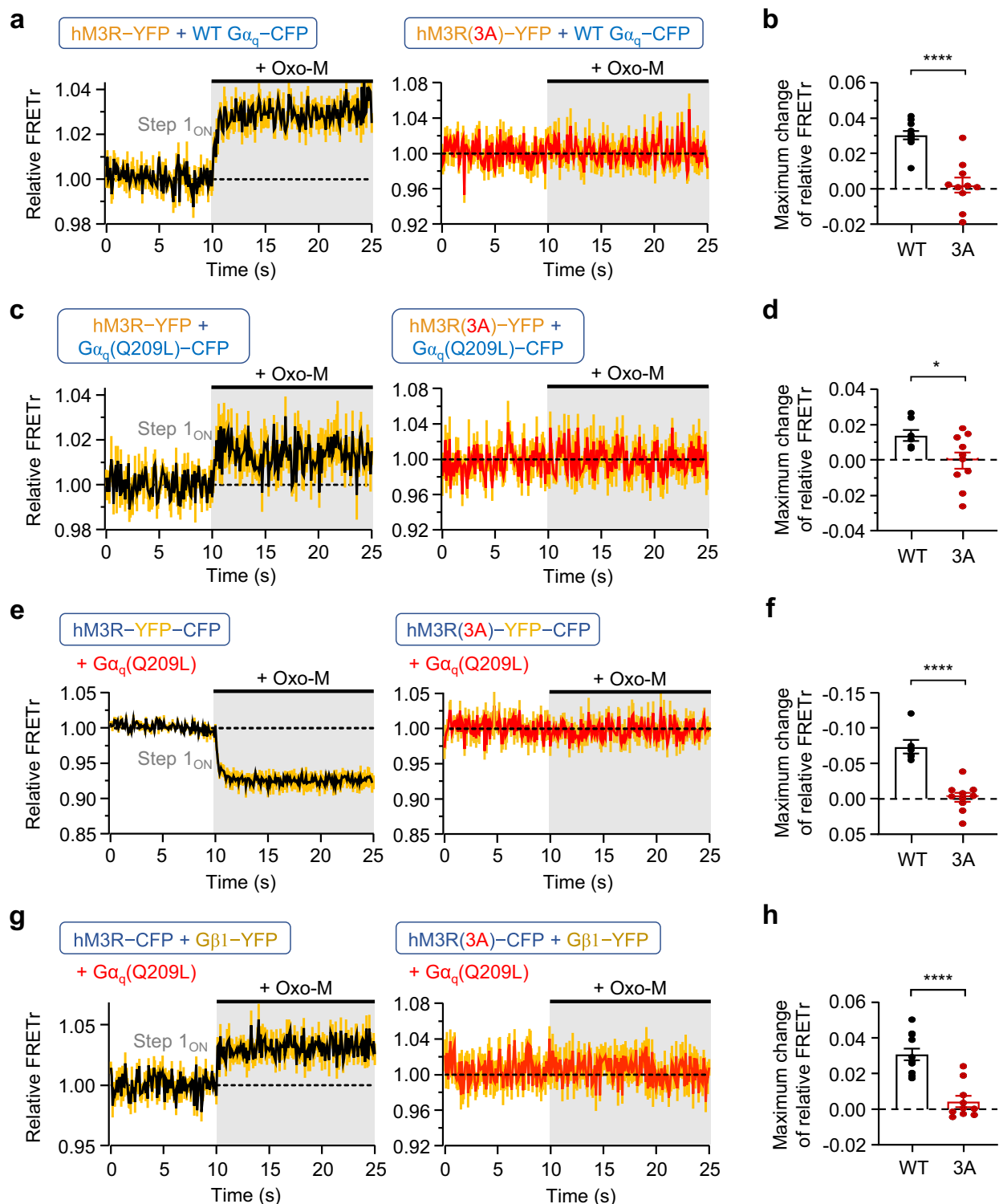
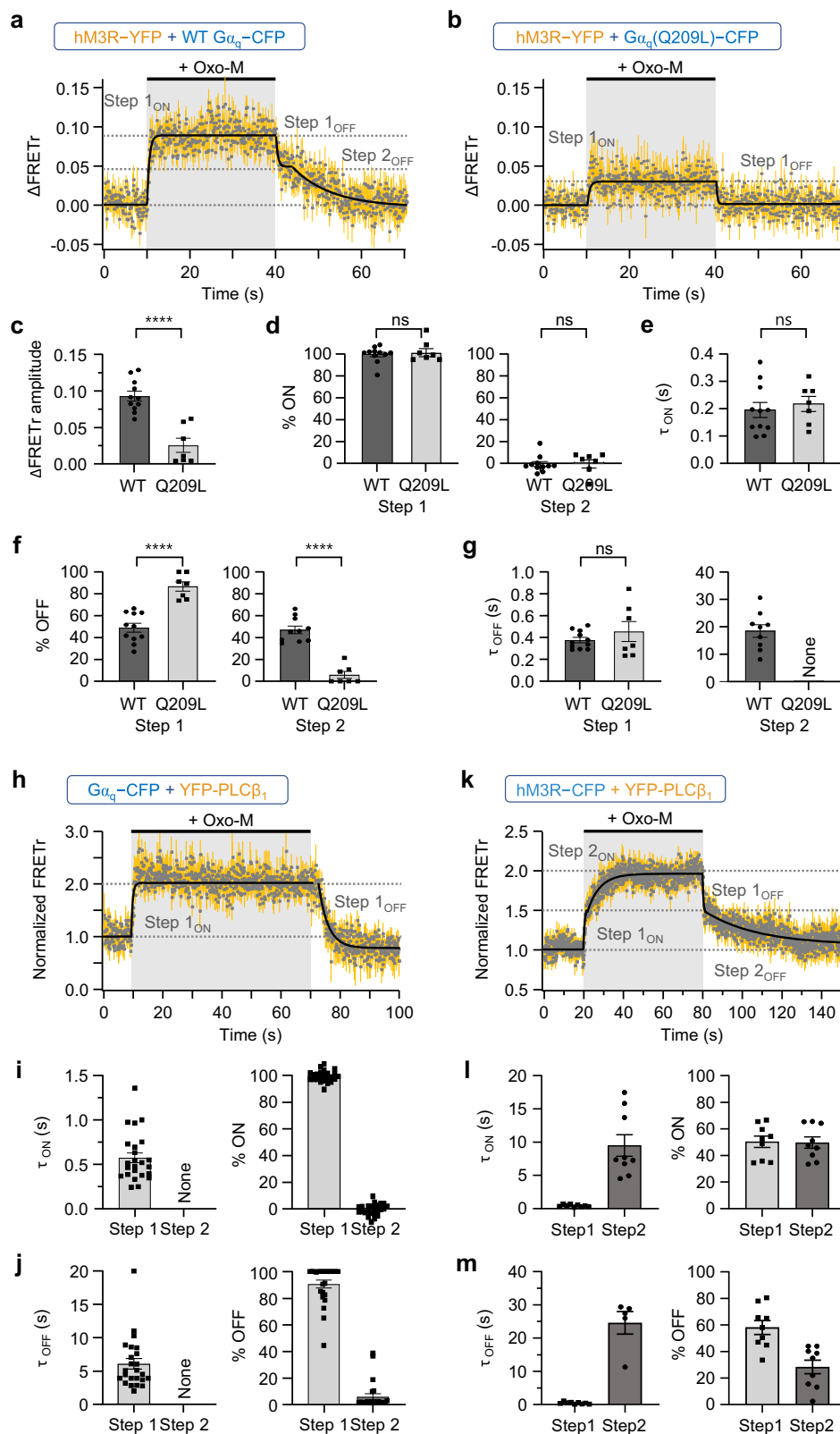


**Fig. 6 | hM3R(3A) does not interact with  $G\beta\gamma$  subunits independently.** **a** Time course of relative FRET in response to 15 s of Oxo-M in cells expressing  $G\alpha_q$ -CFP,  $G\beta 1$ ,  $G\gamma 2$ , and hM3R-YFP (left,  $n = 11$ , two cultures) or hM3R(3A)-YFP (right,  $n = 10$ , two cultures). Sampling frequency: 10 Hz. Yellow vertical lines indicate SEM. **b** Maximum change of relative FRET in cells expressing each FRET sensor by Oxo-M treatment. WT,  $n = 11$  (two cultures); 3A,  $n = 10$  (two cultures). Student's  $t$  test (two-sided, \*\*\*\* $p < 0.0001$ ). **c** Time course of relative FRET in response to 15 s of Oxo-M in cells expressing  $G\alpha_q(Q209L)$ -CFP,  $G\beta 1$ ,  $G\gamma 2$ , and hM3R-YFP (left,  $n = 7$ , two cultures) or hM3R(3A)-YFP (right,  $n = 10$ , two cultures). Sampling frequency: 10 Hz. **d** Maximum change of relative FRET in cells expressing each FRET sensor by Oxo-M treatment. WT,  $n = 7$  (two cultures); 3A,  $n = 10$  (two cultures). Student's  $t$  test (two-sided, \* $p = 0.0352$ ). **e** Time course of relative FRET in response to 15 s of Oxo-

M in cells expressing  $G\alpha_q(Q209L)$ ,  $G\beta 1$ ,  $G\gamma 2$ , and hM3R-YFP-CFP (left,  $n = 6$ , two cultures) or hM3R(3A)-YFP-CFP (right,  $n = 10$ , two cultures). Sampling frequency: 10 Hz. **f** Maximum change of relative FRET in cells expressing each FRET sensor by Oxo-M treatment. WT,  $n = 6$  (two cultures); 3A,  $n = 10$  (two cultures). Student's  $t$  test (two-sided, \*\*\*\* $p < 0.0001$ ). **g** Time course of relative FRET in response to 15 s of Oxo-M in cells expressing  $G\alpha_q(Q209L)$ ,  $G\beta 1$ -YFP,  $G\gamma 2$ , and hM3R-CFP (left,  $n = 11$ , two cultures) or hM3R(3A)-CFP (right,  $n = 10$ , two cultures). Sampling frequency: 10 Hz. **h** Maximum change of relative FRET in cells expressing each FRET sensor by Oxo-M treatment. WT,  $n = 11$  (two cultures); 3A,  $n = 10$  (two cultures). Student's  $t$  test (two-sided, \*\*\*\* $p < 0.0001$ ). Data are shown as mean  $\pm$  SEM, with error bars indicating SEM. Source data are provided as a Source Data file.



Scientific Instruments (Farmingdale, New York). This supplied solution was simultaneously sucked out by the vacuum pump system DR 4-000-007 from Drummond Scientific Company (Broomall, Pennsylvania). The external Ringer's solution exchange for drug treatment was accomplished by a theta tube moved laterally by a step-driven motor (SF-77C) from Warner Instruments (Holliston, Massachusetts) and was complete within 20 ms. The external Ringer's solution used for FRET

and confocal imaging contained the following (in mM): 160 NaCl, 2.5 KCl, 2 CaCl<sub>2</sub>, 1 MgCl<sub>2</sub>, 10 HEPES, and 8 glucose, adjusted to pH 7.4 with NaOH. The pipette solution for FRET under the normal GTP concentration (0.1 mM) condition contained the following (in mM): 175 KCl, 5 MgCl<sub>2</sub>, 5 HEPES, 0.1 BAPTA, 3 Na<sub>2</sub>ATP, and 0.1 Na<sub>3</sub>GTP, adjusted to pH 7.4 with KOH. For the case of the GTP depletion condition, the 0.1 mM Na<sub>3</sub>GTP was substituted with 1 mM GDP $\beta$ S. For the case of the

**Fig. 7 | hM3R,  $G_{\alpha_q}$ , and PLC form a heterotrimer during receptor activation.** Time course of  $\Delta$ FRET<sub>r</sub> in response to 30 s of Oxo-M in cells expressing hM3R-YFP, G $\beta$ 1, G $\gamma$ 2 and wild-type (WT)  $G_{\alpha_q}$ -CFP (a) or  $G_{\alpha_q}$ (Q209L)-CFP (b). Sampling frequency: 10 Hz. Yellow vertical lines indicate SEM. WT,  $n = 11$  (two cultures); Q209L,  $n = 7$  (two cultures). c Amplitude of  $\Delta$ FRET<sub>r</sub> in cells expressing each FRET sensor. WT,  $n = 11$  (two cultures); Q209L,  $n = 7$  (two cultures). Student's  $t$  test (two-sided, \*\*\*\* $p < 0.0001$ ). d Percent distribution of each step in total FRET<sub>r</sub> response. WT,  $n = 11$  (two cultures); Q209L,  $n = 7$  (two cultures). Student's  $t$  test (two-sided). e  $\tau_{ON}$  of step 1<sub>ON</sub>. WT,  $n = 11$  (two cultures); Q209L,  $n = 7$  (two cultures). Student's  $t$  test (two-sided). f Percent of each decreasing step in contrast to step 1<sub>ON</sub>. WT,  $n = 11$  (two cultures); Q209L,  $n = 7$  (two cultures). Student's  $t$  test (two-sided).

\*\*\*\* $p < 0.0001$ . g  $\tau_{OFF}$  of each deactivation step. WT,  $n = 11$  (two cultures); Q209L,  $n = 7$  (two cultures). Welch's  $t$  test (two-sided). h, k Time course of normalized FRET<sub>r</sub> in response to 60 s of Oxo-M in cells expressing hM3R,  $G_{\alpha_q}$ -CFP, G $\beta$ 1, G $\gamma$ 2, and YFP-PLC $\beta_1$  (h,  $n = 24$ , two cultures) or in cells expressing hM3R-CFP, and YFP-PLC $\beta_1$  (k,  $n = 9$ , two cultures). Sampling frequency: 10 Hz. Yellow vertical lines indicate SEM. i, l  $\tau_{ON}$  of each activation step and percent distribution of each step in total FRET<sub>r</sub> response (i,  $n = 24$ , two cultures; l,  $n = 9$ , two cultures). j, m  $\tau_{OFF}$  of each deactivation step and percent of each decreasing step in contrast to total FRET<sub>r</sub> response of activation (j,  $n = 24$ , two cultures; m,  $n = 9$ , two cultures). Data are shown as mean  $\pm$  SEM, with error bars indicating SEM. ns not significant. Source data are provided as a Source Data file.

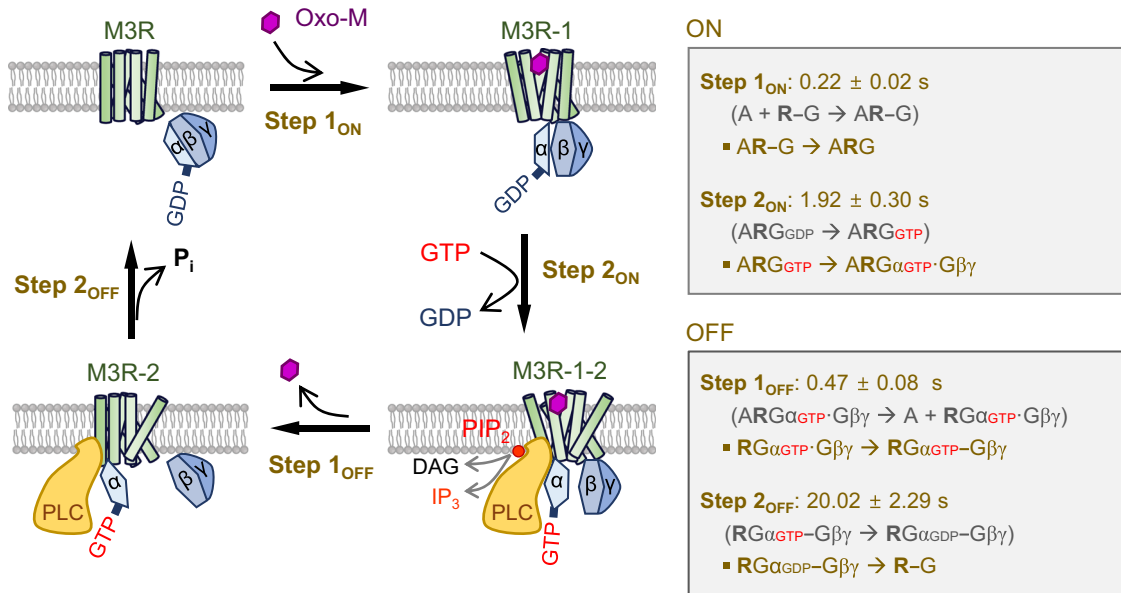


**Fig. 8 | Schematic diagram of  $G_q$  protein cycle-mediated conformational changes of hM3R.** Cartoon depicts the effects of  $G_q$  protein cycle on two-step activation and two-step deactivation of hM3R conformation. Boxes summarized the underlying processes of each step occurring during ON and OFF reactions. The reactions in the parentheses were not observed. The dash line (-) means a status of partial interaction or preassembly and a structural rearrangement by agonist

binding induces more tighter binding. The binding of inactive  $G_q$  protein with the agonist-bound hM3R evokes a slight change in the coupling conformation between  $G_{\alpha_q}$  and  $G\beta\gamma$  subunits. The activated  $G_{\alpha_q}$ -GTP subunit does not dissociate from the ligand-activated hM3R, and it simultaneously stimulates PLC $\beta$  by forming a heteromeric complex.

nonhydrolyzable GTP analog experiments, the 0.1 mM GTP was substituted with 0.1 mM GTP $\gamma$ S. When using Oxo-M as an agonist, a concentration of 10  $\mu$ M was used. Oxo-M, Ach and poly-L-lysine were from Sigma-Aldrich (St. Louis, Missouri). DMEM, Lipofectamine-2000, and penicillin/streptomycin were from Invitrogen (Waltham, Massachusetts). Fetal bovine serum was from Gemini Bio-Products (West Sacramento, California). YM-254890 was from Cayman Chemical (Ann Arbor, Michigan).

#### In silico modeling using I-TASSER and SWISS-Model

For the predicted three-dimensional (3D) structure of M3R with mutating  $G_{\alpha}$ -binding sites, molecular modeling was executed by using the cryo-EM structure of rat M3R (PDB ID: 4DAJ)<sup>53</sup> as a template from Protein Data Bank (PDB) because there is no cryo-EM structure of human M3R. In Swiss-Model, we used the structure with PDB ID: 4U14 determined by X-ray crystallography as template<sup>78</sup>. We submitted the full sequence of rat M3R(3A) (derived from NM\_012527.2) and obtained models predicted from I-TASSER online server V5.2 (<http://zhanglab.ccmb.med.umich.edu/I-TASSER/>)<sup>79</sup> and SWISS-Model web server released from July 2022 (<https://swissmodel.expasy.org/>). Excluding the flexible intracellular loops, transmembrane domains with  $G_{\alpha}$ -binding sites of cryo-EM M3R and in silico M3R(3A) model were superimposed by matchmaker of University of California, San

Francisco (UCSF) chimera. The amino-acid residues representing orthosteric agonist-binding sites<sup>53,80</sup> and  $G_{\alpha}$ -binding sites<sup>48,52</sup> were indicated. Structure visualization and modifications were made using UCSF chimera.

#### Data analysis

All data were analyzed using Excel 2016 (Microsoft), Igor Pro-6.0 (WaveMetrics), or GraphPad Prism 8 (GraphPad Software). The measured FRET<sub>r</sub> traces were normalized as follows. The average FRET<sub>r</sub> signal of 5-s period before the agonist treatment was set to the initial value 1. The average FRET<sub>r</sub> signal of 5-s period before the washing out of drugs was set to the minimum 0 or maximum 2 value according to the direction of the reactions. To measure the relative FRET<sub>r</sub> in a time course, the data at each time point were divided by the average FRET<sub>r</sub> signal of 5-s period before the agonist treatment. To perform a fitting and determine a time constant ( $\tau$ ) and  $\Delta$ FRET<sub>r</sub> amplitude of activation in the “hM3R-YFP-CFP” experiments, when the starting point of agonist treatment was regarded as the zero time point, the time duration from 0 to 1.2 s after agonist addition was designated as “Step 1<sub>ON</sub>” and the 1.3–15 s time period during the agonist treatment was designated as “Step 2<sub>ON</sub>”. To perform a fitting and determine a time constant ( $\tau$ ) of deactivation in the “hM3R-YFP +  $G_{\alpha_q}$ -CFP” experiments, 0–3.6 s was designated as “Step 1<sub>OFF</sub>” and 3.7–30 s was designated as “Step 2<sub>OFF</sub>”.

Except for the cases previously described, a fitting was performed with a least-squares criterion to determine time constants ( $\tau$ ) of activation and deactivation and the maximum  $\Delta$ FRET amplitude. The signal-to-noise ratio (SNR) was calculated as the maximum  $\Delta$ FRET amplitude divided by the standard error of the baseline  $\Delta$ FRET. Percent (%) ON of FRET of hM3R-YFP-CFP was calculated as  $100 \times (\Delta$ FRET amplitude of each activation step (step 1 or step 2)/maximum  $\Delta$ FRET amplitude). Percent (%) ON of FRET of the other constructs with single-step activation was calculated as  $100 \times$  (the average of the amplitudes (in contrast to the initial value 1) of points of 2.5-s period before washing out of agonist in each normalized FRET/the average of the amplitudes (in contrast to the initial value 1) of points of 2.5-s period before agonist washing out in normalized average FRET). Percent (%) OFF of FRET of hM3R-YFP-CFP was calculated as  $100 \times (\Delta$ FRET amplitude of each deactivation step (step 1 or step 2)/maximum  $\Delta$ FRET amplitude of activation). Percent (%) OFF of FRET of the other constructs with single-step deactivation was calculated as  $100 \times (\Delta$ FRET amplitude of deactivation/maximum  $\Delta$ FRET amplitude of activation). Statistics in the text and figures represent mean  $\pm$  SEM. Statistical comparisons between the means of two groups were analyzed using Student's *t*-test and Welch's *t*-test according to their variances. Otherwise, Mann–Whitney *U* test was used if the data did not follow normal distribution. Statistical significances of  $\Delta$ FRET changes before and after receptor activations were analyzed using paired *t*-test. Statistical comparisons between the means of three or more independent groups under one independent variable were analyzed using one-way ANOVA or Welch's ANOVA according to their variances. Statistical comparisons between the means of three or more independent groups with equal variance under two independent variables were analyzed using two-way ANOVA. Differences were considered significant at the  $*P < 0.05$ ,  $**P < 0.01$ ,  $***P < 0.001$ , and  $****P < 0.0001$  levels. Source data used in data analysis are provided with this paper.

### Reporting summary

Further information on research design is available in the Nature Portfolio Reporting Summary linked to this article.

### Data availability

The data that support this study are available from the corresponding authors upon request. The published cryo-EM structure of rat M3R can be accessed using accession code [4DAJ](#). The published X-ray crystal structure of rat M3R can be accessed using accession code [4UI4](#). Source data are provided with this paper.

### References

- Klabunde, T. & Hessler, G. Drug design strategies for targeting G-protein-coupled receptors. *ChemBioChem* **3**, 928–944 (2002).
- Fredriksson, R., Lagerstrom, M. C., Lundin, L. G. & Schiöth, H. B. The G-protein-coupled receptors in the human genome form five main families. Phylogenetic analysis, paralogon groups, and fingerprints. *Mol. Pharmacol.* **63**, 1256–1272 (2003).
- Pin, J. P., Kniazeff, J., Prezeau, L., Liu, J. F. & Rondard, P. GPCR interaction as a possible way for allosteric control between receptors. *Mol. Cell. Endocrinol.* **486**, 89–95 (2019).
- Lagerstrom, M. C. & Schiöth, H. B. Structural diversity of G protein-coupled receptors and significance for drug discovery. *Nat. Rev. Drug Discov.* **7**, 339–357 (2008).
- Calebiro, D., Koszegi, Z., Lanoiselee, Y., Miljus, T. & O'Brien, S. G protein-coupled receptor-G protein interactions: a single-molecule perspective. *Physiol. Rev.* **101**, 857–906 (2021).
- Rybin, V. O., Xu, X., Lisanti, M. P. & Steinberg, S. F. Differential targeting of  $\beta$ -adrenergic receptor subtypes and adenylyl cyclase to cardiomyocyte caveolae. A mechanism to functionally regulate the cAMP signaling pathway. *J. Biol. Chem.* **275**, 41447–41457 (2000).
- Insel, P. A. et al. Compartmentation of G-protein-coupled receptors and their signalling components in lipid rafts and caveolae. *Biochem. Soc. Trans.* **33**, 1131–1134 (2005).
- Sungkaworn, T. et al. Single-molecule imaging reveals receptor-G protein interactions at cell surface hot spots. *Nature* **550**, 543–547 (2017).
- De Lean, A., Stadel, J. M. & Lefkowitz, R. J. A ternary complex model explains the agonist-specific binding properties of the adenylyl cyclase-coupled beta-adrenergic receptor. *J. Biol. Chem.* **255**, 7108–7117 (1980).
- Kjeldgaard, M., Nyborg, J. & Clark, B. F. The GTP binding motif: variations on a theme. *FASEB J.* **10**, 1347–1368 (1996).
- Rasmussen, S. G. et al. Crystal structure of the  $\beta_2$  adrenergic receptor-Gs protein complex. *Nature* **477**, 549–555 (2011).
- Glukhova, A. et al. Rules of engagement: GPCRs and G proteins. *ACS Pharmacol. Transl. Sci.* **1**, 73–83 (2018).
- Wu, G., Benovic, J. L., Hildebrandt, J. D. & Lanier, S. M. Receptor docking sites for G-protein betagamma subunits. Implications for signal regulation. *J. Biol. Chem.* **273**, 7197–7200 (1998).
- Herrmann, R. et al. Sequence of interactions in receptor-G protein coupling. *J. Biol. Chem.* **279**, 24283–24290 (2004).
- Herrmann, R., Heck, M., Henklein, P., Hofmann, K. P. & Ernst, O. P. Signal transfer from GPCRs to G proteins: role of the  $G\alpha$  N-terminal region in rhodopsin-transducin coupling. *J. Biol. Chem.* **281**, 30234–30241 (2006).
- Herrmann, R. et al. Rhodopsin-transducin coupling: role of the  $G\alpha$  C-terminus in nucleotide exchange catalysis. *Vision Res.* **46**, 4582–4593 (2006).
- Oldham, W. M. et al. Mechanism of the receptor-catalyzed activation of heterotrimeric G proteins. *Nat. Struct. Mol. Biol.* **13**, 772–777 (2006).
- Dror, R. O. et al. SIGNAL TRANSDUCTION. Structural basis for nucleotide exchange in heterotrimeric G proteins. *Science* **348**, 1361–1365 (2015).
- Zhang, Y. et al. Cryo-EM structure of the activated GLP-1 receptor in complex with a G protein. *Nature* **546**, 248–253 (2017).
- Liang, Y. L. et al. Phase-plate cryo-EM structure of a class B GPCR-G-protein complex. *Nature* **546**, 118–123 (2017).
- Liang, Y. L. et al. Phase-plate cryo-EM structure of a biased agonist-bound human GLP-1 receptor-Gs complex. *Nature* **555**, 121–125 (2018).
- Garcia-Nafria, J., Lee, Y., Bai, X., Carpenter, B. & Tate, C. G. Cryo-EM structure of the adenosine A2A receptor coupled to an engineered heterotrimeric G protein. *Elife* **7**, e35946 (2018).
- Tsai, C. J. et al. Cryo-EM structure of the rhodopsin- $G\alpha_i$ - $\beta\gamma$  complex reveals binding of the rhodopsin C-terminal tail to the  $G\beta$  subunit. *Elife* **8**, e46041 (2019).
- Maeda, S., Qu, Q., Robertson, M. J., Skiniotis, G. & Kobilka, B. K. Structures of the  $M_1$  and  $M_2$  muscarinic acetylcholine receptor/G-protein complexes. *Science* **364**, 552–557 (2019).
- Garcia-Nafria, J. & Tate, C. G. Cryo-EM structures of GPCRs coupled to  $G_s$ ,  $G_i$  and  $G_o$ . *Mol. Cell. Endocrinol.* **488**, 1–13 (2019).
- Neubig, R. R. Membrane organization in G-protein mechanisms. *FASEB J.* **8**, 939–946 (1994).
- Rebois, R. V. & Hebert, T. E. Protein complexes involved in heptahelical receptor-mediated signal transduction. *Recept. Channels* **9**, 169–194 (2003).
- Hein, P. & Bunemann, M. Coupling mode of receptors and G proteins. *Naunyn Schmiedebergs Arch. Pharmacol.* **379**, 435–443 (2009).
- Bunemann, M., Frank, M. & Lohse, M. J.  $G_i$  protein activation in intact cells involves subunit rearrangement rather than dissociation. *Proc. Natl Acad. Sci. USA* **100**, 16077–16082 (2003).
- Gales, C. et al. Real-time monitoring of receptor and G-protein interactions in living cells. *Nat. Methods* **2**, 177–184 (2005).



31. Nobles, M., Benians, A. & Tinker, A. Heterotrimeric G proteins pre-couple with G protein-coupled receptors in living cells. *Proc. Natl Acad. Sci. USA* **102**, 18706–18711 (2005).
32. Gales, C. et al. Probing the activation-promoted structural rearrangements in preassembled receptor-G protein complexes. *Nat. Struct. Mol. Biol.* **13**, 778–786 (2006).
33. Qin, K., Dong, C., Wu, G. & Lambert, N. A. Inactive-state pre-assembly of G<sub>q</sub>-coupled receptors and G<sub>q</sub> heterotrimers. *Nat. Chem. Biol.* **7**, 740–747 (2011).
34. Huang, S. K. et al. Delineating the conformational landscape of the adenosine A<sub>2A</sub> receptor during G protein coupling. *Cell* **184**, 1884–1894.e1814 (2021).
35. Gregorio, G. G. et al. Single-molecule analysis of ligand efficacy in β<sub>2</sub> AR-G-protein activation. *Nature* **547**, 68–73 (2017).
36. Jensen, J. B., Lyssand, J. S., Hague, C. & Hille, B. Fluorescence changes reveal kinetic steps of muscarinic receptor-mediated modulation of phosphoinositides and Kv7.2/7.3 K<sup>+</sup> channels. *J. Gen. Physiol.* **133**, 347–359 (2009).
37. Ziegler, N., Batz, J., Zabel, U., Lohse, M. J. & Hoffmann, C. FRET-based sensors for the human M<sub>1</sub>-, M<sub>3</sub>-, and M<sub>5</sub>-acetylcholine receptors. *Bioorg. Med. Chem.* **19**, 1048–1054 (2011).
38. Hoffmann, C. et al. Comparison of the activation kinetics of the M<sub>3</sub> acetylcholine receptor and a constitutively active mutant receptor in living cells. *Mol. Pharmacol.* **82**, 236–245 (2012).
39. Wolters, V., Krasel, C., Brockmann, J. & Bunemann, M. Influence of Gα<sub>q</sub> on the dynamics of M<sub>3</sub>-acetylcholine receptor-G-protein-coupled receptor kinase 2 interaction. *Mol. Pharmacol.* **87**, 9–17 (2015).
40. Floser, A. et al. Disentangling bias between G<sub>q</sub>, GRK2, and arrestin3 recruitment to the M<sub>3</sub> muscarinic acetylcholine receptor. *Elife* **10**, e58442 (2021).
41. Van Raamsdonk, C. D. et al. Frequent somatic mutations of GNAQ in uveal melanoma and blue naevi. *Nature* **457**, 599–602 (2009).
42. Van Raamsdonk, C. D. et al. Mutations in GNA11 in uveal melanoma. *N. Engl. J. Med.* **363**, 2191–2199 (2010).
43. Campbell, A. P. & Smrcka, A. V. Targeting G protein-coupled receptor signalling by blocking G proteins. *Nat. Rev. Drug Discov.* **17**, 789–803 (2018).
44. Harrison, C. & Traynor, J. R. The [<sup>35</sup>S]GTPγS binding assay: approaches and applications in pharmacology. *Life Sci.* **74**, 489–508 (2003).
45. Jing, M. et al. An optimized acetylcholine sensor for monitoring in vivo cholinergic activity. *Nat. Methods* **17**, 1139–1146 (2020).
46. Jing, M. et al. A genetically encoded fluorescent acetylcholine indicator for in vitro and in vivo studies. *Nat. Biotechnol.* **36**, 726–737 (2018).
47. Tateyama, M. & Kubo, Y. Analyses of the effects of Gq protein on the activated states of the muscarinic M<sub>3</sub> receptor and the purinergic P2Y<sub>1</sub> receptor. *Physiol. Rep.* **1**, e00134 (2013).
48. Venkatakrishnan, A. J. et al. Diverse activation pathways in class A GPCRs converge near the G-protein-coupling region. *Nature* **536**, 484–487 (2016).
49. Isberg, V. et al. Generic GPCR residue numbers - aligning topology maps while minding the gaps. *Trends Pharmacol. Sci.* **36**, 22–31 (2015).
50. Isberg, V. et al. GPCRdb: an information system for G protein-coupled receptors. *Nucleic Acids Res.* **44**, D356–D364 (2016).
51. Flock, T. et al. Universal allosteric mechanism for Gα activation by GPCRs. *Nature* **524**, 173–179 (2015).
52. Liu, Q. et al. Ligand recognition and G-protein coupling selectivity of cholecystokinin A receptor. *Nat. Chem. Biol.* **17**, 1238–1244 (2021).
53. Kruse, A. C. et al. Structure and dynamics of the M3 muscarinic acetylcholine receptor. *Nature* **482**, 552–556 (2012).
54. Nakajima, K. & Wess, J. Design and functional characterization of a novel, arrestin-biased designer G protein-coupled receptor. *Mol. Pharmacol.* **82**, 575–582 (2012).
55. Hein, P. et al. G<sub>s</sub> activation is time-limiting in initiating receptor-mediated signaling. *J. Biol. Chem.* **281**, 33345–33351 (2006).
56. Rochais, F. et al. Real-time optical recording of β<sub>1</sub>-adrenergic receptor activation reveals supersensitivity of the Arg389 variant to carvedilol. *J. Clin. Investig.* **117**, 229–235 (2007).
57. Ferrandon, S. et al. Sustained cyclic AMP production by parathyroid hormone receptor endocytosis. *Nat. Chem. Biol.* **5**, 734–742 (2009).
58. Reiner, S., Ambrosio, M., Hoffmann, C. & Lohse, M. J. Differential signaling of the endogenous agonists at the β<sub>2</sub>-adrenergic receptor. *J. Biol. Chem.* **285**, 36188–36198 (2010).
59. Sleno, R. et al. Designing BRET-based conformational biosensors for G protein-coupled receptors. *Methods* **92**, 11–18 (2016).
60. Bourque, K. et al. Distinct conformational dynamics of three G protein-coupled receptors measured using FLASH-BRET biosensors. *Front. Endocrinol.* **8**, 61 (2017).
61. Che, T. et al. Nanobody-enabled monitoring of kappa opioid receptor states. *Nat. Commun.* **11**, 1145 (2020).
62. Lohse, M. J., Nuber, S. & Hoffmann, C. Fluorescence/bioluminescence resonance energy transfer techniques to study G-protein-coupled receptor activation and signaling. *Pharmacol. Rev.* **64**, 299–336 (2012).
63. Zhou, Y., Meng, J., Xu, C. & Liu, J. Multiple GPCR functional assays based on resonance energy transfer sensors. *Front. Cell Dev. Biol.* **9**, 611443 (2021).
64. Wess, J. Molecular basis of receptor/G-protein-coupling selectivity. *Pharmacol. Ther.* **80**, 231–264 (1998).
65. Azpiazu, I. & Gautam, N. A fluorescence resonance energy transfer-based sensor indicates that receptor access to a G protein is unrestricted in a living mammalian cell. *J. Biol. Chem.* **279**, 27709–27718 (2004).
66. Davare, M. A. et al. A β<sub>2</sub> adrenergic receptor signaling complex assembled with the Ca<sup>2+</sup> channel Ca<sub>v</sub>1.2. *Science* **293**, 98–101 (2001).
67. Rebois, R. V. et al. Heterotrimeric G proteins form stable complexes with adenylyl cyclase and Kir3.1 channels in living cells. *J. Cell Sci.* **119**, 2807–2818 (2006).
68. Halls, M. L. & Cooper, D. M. Sub-picomolar relaxin signalling by a pre-assembled RXFP1, AKAP79, AC2, β-arrestin 2, PDE4D3 complex. *EMBO J.* **29**, 2772–2787 (2010).
69. Nagi, K. & Peineyro, G. Kir3 channel signaling complexes: focus on opioid receptor signaling. *Front. Cell. Neurosci.* **8**, 186 (2014).
70. Kankanamge, D. et al. Dissociation of the G protein betagamma from the G<sub>q</sub>-PLCβ complex partially attenuates PIP<sub>2</sub> hydrolysis. *J. Biol. Chem.* **296**, 100702 (2021).
71. Hughes, T. E., Zhang, H., Logothetis, D. E. & Berlot, C. H. Visualization of a functional Gα<sub>q</sub>-green fluorescent protein fusion in living cells. Association with the plasma membrane is disrupted by mutational activation and by elimination of palmitoylation sites, but not by activation mediated by receptors or AIF4. *J. Biol. Chem.* **276**, 4227–4235 (2001).
72. Scarlata, S. & Dowal, L. The use of green fluorescent proteins to view association between phospholipase C beta and G protein subunits in cells. *Methods Mol. Biol.* **237**, 223–232 (2004).
73. Suh, B. C., Inoue, T., Meyer, T. & Hille, B. Rapid chemically induced changes of PtdIns(4,5)P<sub>2</sub> gate KCNQ ion channels. *Science* **314**, 1454–1457 (2006).
74. van der Wal, J., Habets, R., Varnai, P., Balla, T. & Jalink, K. Monitoring agonist-induced phospholipase C activation in live cells by fluorescence resonance energy transfer. *J. Biol. Chem.* **276**, 15337–15344 (2001).
75. Keum, D., Baek, C., Kim, D. I., Kweon, H. J. & Suh, B. C. Voltage-dependent regulation of Ca<sub>v</sub>2.2 channels by G<sub>q</sub>-coupled receptor is

- facilitated by membrane-localized  $\beta$  subunit. *J. Gen. Physiol* **144**, 297–309 (2014).
76. Keum, D., Kruse, M., Kim, D. I., Hille, B. & Suh, B. C. Phosphoinositide 5- and 3-phosphatase activities of a voltage-sensing phosphatase in living cells show identical voltage dependence. *Proc. Natl Acad. Sci. USA* **113**, E3686–E3695 (2016).
77. Park, C. G., Yu, W. & Suh, B. C. Molecular basis of the  $\text{PIP}_2$ -dependent regulation of  $\text{Ca}_v2.2$  channel and its modulation by  $\text{Ca}_v$   $\beta$  subunits. *Elife* **11**, e69500 (2022).
78. Thorsen, T. S., Matt, R., Weis, W. I. & Kobilka, B. K. Modified T4 lysozyme fusion proteins facilitate G protein-coupled receptor crystallogenesis. *Structure* **22**, 1657–1664 (2014).
79. Yang, J. & Zhang, Y. I-TASSER server: new development for protein structure and function predictions. *Nucleic Acids Res.* **43**, W174–W181 (2015).
80. Levay, M. et al. NSC23766, a widely used inhibitor of Rac1 activation, additionally acts as a competitive antagonist at muscarinic acetylcholine receptors. *J. Pharmacol. Exp. Ther.* **347**, 69–79 (2013).

## Acknowledgements

We thank the many laboratories that kindly provided the plasmids. This work was supported by the National Research Foundation of Korea (NRF) grant funded by the Korea government (Ministry of Science, Information and Communications Technology, and Future Planning) (2022R1A2C1006560 [B.-C.S.]) and the Basic Science Research Program (2020R1A4A1019436 [B.-C.S.]).

## Author contributions

B.-C.S. and Y.-S.K. conceptualized the project and designed the experiments; Y.-S.K. performed most of the experiments; J.-H.Y. performed amino-acid point mutations to construct the hM3R(3A) expression vectors and the hM3R(R166L<sup>3x50</sup>)-YFP-CFP expression vector; W.K. performed In silico modelling using I-TASSER and SWISS-Model; Y.-S.K. analyzed the results; Y.-S.K. wrote the original draft. All authors edited the manuscript. B.-C.S. supervised the project and wrote the final paper.

## Competing interests

Y.-S.K. and B.-C.S. have a pending patent for hM3R-YFP-CFP and use there of: South Korean patent application number 10-2022-0147739. The other authors declare no competing interests.

## Additional information

**Supplementary information** The online version contains supplementary material available at <https://doi.org/10.1038/s41467-023-36911-4>.

**Correspondence** and requests for materials should be addressed to Byung-Chang Suh.

**Peer review information** *Nature Communications* thanks the anonymous reviewers for their contribution to the peer review of this work.

**Reprints and permissions information** is available at <http://www.nature.com/reprints>

**Publisher's note** Springer Nature remains neutral with regard to jurisdictional claims in published maps and institutional affiliations.

**Open Access** This article is licensed under a Creative Commons Attribution 4.0 International License, which permits use, sharing, adaptation, distribution and reproduction in any medium or format, as long as you give appropriate credit to the original author(s) and the source, provide a link to the Creative Commons license, and indicate if changes were made. The images or other third party material in this article are included in the article's Creative Commons license, unless indicated otherwise in a credit line to the material. If material is not included in the article's Creative Commons license and your intended use is not permitted by statutory regulation or exceeds the permitted use, you will need to obtain permission directly from the copyright holder. To view a copy of this license, visit <http://creativecommons.org/licenses/by/4.0/>.

© The Author(s) 2023